REPORT NO.
UCB/SEMM-93/03

STRUCTURAL ENGINEERING,
MECHANICS AND MATERIALS

TWO MATERIAL MODELS FOR CYCLIC PLASTICITY: NON-LINEAR KINEMATIC HARDENING AND GENERALIZED PLASTICITY

by

FERDINANDO AURICCHIO

and

ROBERT L. TAYLOR

FEB 1993

DEPARTMENT OF CIVIL ENGINEERING
UNIVERSITY OF CALIFORNIA
BERKELEY, CALIFORNIA

TWO MATERIAL MODELS FOR CYCLIC PLASTICITY: NON-LINEAR KINEMATIC HARDENING AND GENERALIZED PLASTICITY

F.Auricchio R.L.Taylor
Department of Civil Engineering
University of California at Berkeley, Berkeley, CA 94720 USA

Contents

Abstract

Plasticity models are commonly used to represent the behavior of real materials subjected to extreme loading conditions. Classical plasticity involves a set of linear incremental relations and hardening may be included as an isotropic or a kinematic model. Many finite element implementations for plasticity use linear or piece-wise linear hardening rules, which do not lead to accurate representations of experiments on real materials, especially under cyclic loading conditions.

To generate more realistic constitutive models, a non-linear stress-strain relation is needed. In this paper we focus on two different methods that may be adopted to achieve this goal: the first is based on a *non-linear kinematic hardening* mechanism; the second on a non-linear plastic strain constitutive equation, as given by a *generalized plasticity* model.

The two models are reviewed and discussed from both a continuous and a discrete time point of view. Their implementation in the realm of a radial return mapping algorithm is also addressed. The form of the elasto-plastic tangent tensor consistent with the continuous and the discrete models is discussed; in particular, the latter guarantees quadratic convergence for a Newton method, frequently adopted in the incremental solution of finite element schemes. Finally, some numerical examples for uni-axial and multi-axial (tension-shear) cyclic loading condition under displacement and load control are presented.

1 INTRODUCTION

In one of its most widely used forms, the plasticity theory involves a linear incremental relation between the stress and the plastic strain; moreover, it allows only for linear or piece-wise linear hardening mechanisms. Accordingly, it shows the well known piece-wise linear elasto-plastic stress-strain relation, which is far from being able to simulate experiments on real materials, especially under cyclic loading conditions. Hence, some modifications should be made to improve this model, to which we refer as *classical plasticity.*

Many authors have tried to design material models, showing more realistic non-linear stress-strain relations. We would like to cite few of them: Phillips, Eisenberg and Sierakowski [40, 42, 17, 18, 16], Lubahn [27] Armstrong and Frederick [1] Mroz [34, 35, 36], Dafalias and Popov [12, 13, 10, 11], Lamba and Sidebottom [24, 25], Drucker and Palgen [15], Naghdi and Nikkel [37], McDowell [32, 33], Hassam and Kyriakides [21, 20], Chaboche et al. [4, 5, 7, 8, 6, 9] Chaboche and Lemaitre [26], Doghri [14], Lubliner [29], Lubliner, Taylor and Auricchio [30, 3]. In the cited literature, two basic methods are adopted to generate realistic constitutive theories: the first approach is based on the use of sophisticated (non-linear and/or non-associative) kinematic hardening rules; the second approach is based on the use of non-linear evolutionary equations for the plastic strain in terms of the stress. In the present paper, we focus on two specific models: a *non-linear kinematic hardening* model within the first approach [1, 5] and a *generalized plasticity* model within the second approach [30, 3].

The paper is organized as follow. In Section 2, after recalling our definition for an inelastic body within an internal variable plasticity theory, we present the hypothesis underlying the paper, which mainly are an associative flow rule and a $J2$ material. In Sections 3 and 4 we study from a continuous and a discrete time point of view any material model fitting within the framework of Section 2, outlining also an algorithmic implementation within a radial return mapping algorithm. The forms of the elasto-plastic tensor consistent with the continuous and the discrete model are presented. Thereafter, we specialize the discussion to three specific material models: classical plasticity (CP), non-linear kinematic hardening plasticity (NLK) and generalized plasticity (GP). Each one is analyzed from both a continuous and a discrete point of view and particular attention is paid to their algorithmic implementation; the consistent continuous and discrete elasto-plastic tensors

are also addressed for each model. Specialization of the models to the case of uni-axial states is briefly discussed in Section 8. We conclude the paper with some numerical examples for uni-axial and multi-axial cyclic loading condition under displacement and load control.

We would like to close this introduction stressing that the discussion is restricted to the realm of plasticity (i.e. to theories with a yield surface) and this is the reason for omitting so far any reference to another fruitful approach for the development of constitutive models, the *endochronic theory.* Introduced originally by Valanis in 1971 [47, 48] and with a major modification in 1980 [49], the endochronic theory is based on an intrinsic time, related to the deformation history of the material point, the relation being a material property. In its general form, the theory does not require the existence of a yield function, which however can be obtained by introducing a Dirac delta function. Within this approach, as discussed by Watanabe and Atluri [51, 50] and by Engelstad et al. [19], a kinematic hardening rule can be derived in the form of a hereditary integral. Expressed in differential form, this rule closely resembles the non-linear hardening rule proposed by Armstrong and Frederick [1]. Therefore, our discussion of the NLK model may be easily extended to include this special case of the endochronic theory.

2 BASIC ASSUMPTIONS

In this section, after recalling our definition for an inelastic body within an internal variable plasticity theory, we present the hypothesis underlying the paper, which mainly are an associative flow rule and a $J2$ material.

An *inelastic body* is one in which the strain is determined by the stress and by some additional variables, usually named *internal* or *hidden* [28]. We assume that the inelastic behavior can be treated within the framework of a general plasticity theory, as described in Reference [29]. Accordingly, there exists a continuous *yield function* f, which separates the *elastic* region (for which $f < 0$ and no inelastic effects are present) from the *plastic* region (for which $f \geq 0$ and inelastic deformations occur); furthermore, there exists a continuous *limit function* F, which delimits the domain of all admissible stress states (a stress is admissible only if $F \leq 0$). [1] In our analysis, we do

[1] The yield function f and the limit function F are assumed to be defined in stress space, but corresponding surfaces in strain space can be easily constructed as shown in

not require that the limit function F and the yield function f coincide.

Confining the discussion to a small deformation regime, at any time t the strain $\boldsymbol{\epsilon}$ may be additively decomposed into an elastic and a plastic part, $\boldsymbol{\epsilon}^e$ and $\boldsymbol{\epsilon}^p$ respectively:

$$\boldsymbol{\epsilon} = \boldsymbol{\epsilon}^e + \boldsymbol{\epsilon}^p \tag{2.1}$$

where $\boldsymbol{\epsilon}^e$ can be computed in terms of the stress only:

$$\boldsymbol{\epsilon}^e = \mathbf{C}^{-1}\boldsymbol{\sigma} \tag{2.2}$$

$\mathbf{C}$ being the fourth order elastic modulus tensor. By convention, to simplify the notation, the dependence of the variables on the time t is not explicitly stated. For a linear elastic response, $\mathbf{C}$ is independent of strain.

The internal variables are assumed to be the plastic strain $\boldsymbol{\epsilon}^p$, the back stress $\boldsymbol{\alpha}$ and the accumulative plastic strain $\bar{e}^p$. The back stress $\boldsymbol{\alpha}$ represents the location of the center of the yield surface, which may shift as a result of the kinematic hardening mechanism, while $\bar{e}^p$ is an accumulative measure of the plastic strain, used here to model an isotropic hardening mechanism. The presence of additional variables requires additional constitutive equations, that for now we express in the form:

$$\begin{aligned}
\dot{\boldsymbol{\epsilon}}^p &= \mathbf{g}\left(\boldsymbol{\sigma}, \boldsymbol{\epsilon}^p, \boldsymbol{\alpha}, \bar{e}^p\right) \\
\dot{\bar{e}}^p &= e\left(\boldsymbol{\sigma}, \boldsymbol{\epsilon}^p, \boldsymbol{\alpha}, \bar{e}^p\right) \\
\dot{\boldsymbol{\alpha}} &= \mathbf{h}\left(\boldsymbol{\sigma}, \boldsymbol{\epsilon}^p, \boldsymbol{\alpha}, \bar{e}^p\right)
\end{aligned}$$

where a superpose dot indicates a time derivative. Further, we assume the existence of a flow potential g, function of the stress, such that:

$$\dot{\boldsymbol{\epsilon}}^p = \dot{\gamma}\frac{\partial g}{\partial \boldsymbol{\sigma}}$$

The $\dot{\gamma}$ is a non negative scalar quantity, embodying the plastic rate characteristic of the material and is called the *consistency parameter*, since it is computed requiring the satisfaction of a specific plasticity model. According to the existence of an elastic region, we require:

$$\begin{aligned}
\dot{\gamma} &= 0 \quad when \quad f < 0 \\
\dot{\gamma} &\geq 0 \quad when \quad f \geq 0
\end{aligned}$$

References [39] and [22].

Furthermore, we consider only the case of a flow rule associated with the yield function f, or briefly an associative flow rule; as a result, $g = f$ and:

$$\dot{\boldsymbol{\epsilon}}^p = \dot{\gamma} \frac{\partial f}{\partial \boldsymbol{\sigma}}$$

Consequently, the governing equations are:

$$\boldsymbol{\sigma} = \mathbf{C}\boldsymbol{\epsilon}^e = \mathbf{C}\left[\boldsymbol{\epsilon} - \boldsymbol{\epsilon}^p\right] \tag{2.3}$$

$$\boldsymbol{\Sigma} = \boldsymbol{\sigma} - \boldsymbol{\alpha} \tag{2.4}$$

$$f = f\left(\boldsymbol{\sigma}, \boldsymbol{\epsilon}^p, \boldsymbol{\alpha}, \bar{e}^p\right) \tag{2.5}$$

$$F = F\left(\boldsymbol{\sigma}, \boldsymbol{\epsilon}^p, \boldsymbol{\alpha}, \bar{e}^p, f, \dot{\gamma}\right) \tag{2.6}$$

$$\dot{\boldsymbol{\epsilon}}^p = \dot{\gamma} \frac{\partial f}{\partial \boldsymbol{\sigma}} \tag{2.7}$$

$$\dot{\bar{e}}^p = e\left(\boldsymbol{\sigma}, \boldsymbol{\epsilon}^p, \boldsymbol{\alpha}, \bar{e}^p\right) \tag{2.8}$$

$$\dot{\boldsymbol{\alpha}} = \mathbf{h}\left(\boldsymbol{\sigma}, \boldsymbol{\epsilon}^p, \boldsymbol{\alpha}, \bar{e}^p\right) \tag{2.9}$$

$$\dot{\gamma} \geq 0 \ , \ F \leq 0 \ , \ \dot{\gamma} F = 0 \tag{2.10}$$

where:

- Equation 2.3 is the linear elastic relation between the stress $\boldsymbol{\sigma}$ and the elastic strain $\boldsymbol{\epsilon}^e$, which is also expressed in terms of total and plastic strain by the additive decomposition presented in equation 2.1.
- Equation 2.4 is merely the definition of the *relative* stress $\boldsymbol{\Sigma}$.
- Equation 2.5 is the yield function, where an explicit dependence on the stress, the plastic strain and the back stress is stated. Further, a dependence on the scalar accumulative measure of the plastic strain, $\bar{e}^p$, is included to model an isotropic hardening mechanism.
- Equation 2.6 is the limit function, which may explicitly depend also on the yield function f and the consistency parameter $\dot{\gamma}$. Observe once more that the functions F and f are not required to be the same, although they may coincide for some specific model, such as classical plasticity.
- Equation 2.7 is the constitutive equation (flow rule) for the plastic strain, in the framework of associative plasticity.

- Equation 2.8 is the constitutive equation for the accumulative plastic strain $\bar{e}^p$.
- Equation 2.9 is the constitutive equation for the kinematic hardening mechanism.
- Equations 2.10 are the Kuhn-Tucker conditions, which reduce the plastic problem to a constrained optimization problem.

Finally, we limit our discussion to the case of isotropic materials whose inelastic behavior is controlled only by the second invariant of the deviatoric stress, J_2, and we shall refer to this general class as von Mises or J2 materials. Accordingly, the evolution equations involve only the deviatoric stress and strain, $\mathbf{s}$ and $\mathbf{e}$ respectively, given by:

$$\begin{aligned} \mathbf{s} &= \boldsymbol{\sigma} - \frac{1}{3}\mathrm{tr}(\boldsymbol{\sigma})\mathbf{1} \\ \mathbf{e} &= \boldsymbol{\epsilon} - \frac{1}{3}\mathrm{tr}(\boldsymbol{\epsilon})\,\mathbf{1} \end{aligned}$$

$\mathbf{1}$ being the second order identity tensor and $\mathrm{tr}(\cdot)$ the trace operator. We note that:

$$\|\mathbf{s}\| = \sqrt{2J_2}$$

since the linear vector space of second order tensors is equipped with the natural (Euclidean) inner product, defined by the trace of the product:

$$\|\mathbf{a}\| = [\mathbf{a} : \mathbf{a}]^{\frac{1}{2}} = [\mathrm{tr}(\mathbf{a} \cdot \mathbf{a})]^{\frac{1}{2}}$$

$\mathbf{a}$ being any second order tensor; moreover:

$$\frac{\partial \|\mathbf{a}\|}{\partial \mathbf{a}} = \frac{\mathbf{a}}{\|\mathbf{a}\|} = \bar{\mathbf{a}} \quad , \quad \|\bar{\mathbf{a}}\| = 1$$

Due to the assumption of J2 material and excluding a direct dependence of the yield and the limit functions on the plastic strain, the governing equations

reduce to:

$$p = K\,\theta \tag{2.11}$$

$$\mathbf{s} = 2G\mathbf{e}^e = 2G\,[\mathbf{e} - \mathbf{e}^p] \tag{2.12}$$

$$\boldsymbol{\Sigma} = \mathbf{s} - \boldsymbol{\alpha} \tag{2.13}$$

$$f = f\,(\boldsymbol{\Sigma}, \bar{e}^p) = \|\boldsymbol{\Sigma}\| - \sigma_y(\bar{e}^p) \tag{2.14}$$

$$F = F\,(\boldsymbol{\Sigma}, \bar{e}^p, f, \dot{\gamma}) \tag{2.15}$$

$$\dot{\mathbf{e}}^p = \dot{\gamma}\frac{\partial f}{\partial \boldsymbol{\sigma}} = \dot{\gamma}\frac{\partial f}{\partial \boldsymbol{\Sigma}} = \dot{\gamma}\,\mathbf{n} \tag{2.16}$$

$$\dot{\bar{e}}^p = \|\dot{\mathbf{e}}^p\| \tag{2.17}$$

$$\dot{\boldsymbol{\alpha}} = H_{kin}\dot{\mathbf{e}}^p - H_{nl}\dot{\bar{e}}^p\boldsymbol{\alpha} \tag{2.18}$$

$$\dot{\gamma} \geq 0 \ , \ F \leq 0 \ , \ \dot{\gamma}F = 0 \tag{2.19}$$

where:

- Equation 2.11 is the linear elastic relation between the volumetric part of the stress (the pressure $p = \mathrm{tr}(\boldsymbol{\sigma})/3$) and the volumetric part of the strain ($\theta = \mathrm{tr}(\boldsymbol{\epsilon})$), K being the bulk modulus.

- Equation 2.12 is the linear elastic relation between the deviatoric stress $\mathbf{s}$ and the elastic deviatoric strain $\mathbf{e}^e$, which involves the shear modulus G; $\mathbf{e}$ and $\mathbf{e}^p$ are respectively the deviatoric part of the total and the plastic strain.

- Equation 2.13 is the *relative* stress $\boldsymbol{\Sigma}$, in terms of the deviatoric stress $\mathbf{s}$ and the deviatoric back stress $\boldsymbol{\alpha}$.

- Equation 2.14 is the von Mises yield function, expressed in terms of the relative stress norm and the radius of the yield surface σ_y. The radius of the yield function is variable in time, due to an isotropic hardening mechanism, which is given in the simplest form by:

  $$\sigma_y = \sigma_{y,0} + H_{iso}\,\bar{e}^p \tag{2.20}$$

  $\sigma_{y,0}$ being the initial yield stress.

- Equation 2.15 is the limit function.

- Equation 2.16 is the constitutive equation for the deviatoric plastic strain. We note that, due to the specific form of the yield function f, the tensor $\mathbf{n}$ normal to f has unit norm.

- Equation 2.17 is the constitutive equation for the accumulative plastic strain $\bar{e}^p$ and using equation 2.16 it can be rewritten as:

  $$\dot{\bar{e}}^p = \dot{\gamma} \tag{2.21}$$

- Equation 2.18 is the constitutive equation for the kinematic hardening mechanism. Note that, starting from the general equation 2.9, we restrict its form, still allowing for a non-associative non-linear rule, as the one proposed by Armstrong and Frederick in Reference [1]. Moreover, note that equation 2.18 can be rewritten as:

  $$\dot{\boldsymbol{\alpha}} = H_{kin}\dot{\gamma}\mathbf{n} - H_{nl}\dot{\gamma}\boldsymbol{\alpha} \tag{2.22}$$

  taking advantage of equations 2.16 and 2.21.

- Equations 2.19 are the Kuhn-Tucker conditions.

In Sections 5,6 and 7 we consider three specific material models, which fit within the above general framework. They differ in terms of the limit functions and of the kinematic hardening rules, as summarized in Table 1. For the generalized plasticity model $h(f)$ is a non-linear function, discussed in Section 7. Specialization of the models to uni-axial states is briefly discussed in Section 8.

Material model	Limit function	Kinematic mech.
Classical plasticity (CP)	$F = f = \|\|\boldsymbol{\Sigma}\|\| - \sigma_y$	$\dot{\boldsymbol{\alpha}} = H_{kin}\dot{\gamma}\mathbf{n}$, $H_{nl} = 0$
Non-linear kin.hard.(NLK)	$F = f = \|\|\boldsymbol{\Sigma}\|\| - \sigma_y$	$\dot{\boldsymbol{\alpha}} = H_{kin}\dot{\gamma}\mathbf{n} - H_{nl}\dot{\gamma}\boldsymbol{\alpha}$
Generalized plasticity (GP)	$F = h(f)\,[\mathbf{n} : \dot{\boldsymbol{\sigma}}] - \dot{\gamma}$	$\dot{\boldsymbol{\alpha}} = H_{kin}\dot{\gamma}\mathbf{n}$, $H_{nl} = 0$

Table 1: Limit functions and kinematic mechanisms for the material models discussed

3 CONTINUOUS TIME MODEL

In this section we discuss from a continuous time point of view any material model fitting in the framework presented in Section 2.

3.1 Continuous constitutive equation for the plastic strain

Recalling equation 2.16, the evolution of the plastic strain is governed by:

$$\dot{\mathbf{e}}^p = \dot{\gamma}\mathbf{n}$$

where the unit tensor $\mathbf{n}$ and the scalar parameter $\dot{\gamma}$ provide the direction and the magnitude of the plastic flow, respectively. Given a yield function f and a state of stress, the tensor $\mathbf{n}$ is uniquely determined, while the $\dot{\gamma}$ must be computed by requiring the satisfaction of the limit equation. We assume that the consistency parameter may be expressed as:

$$\dot{\gamma} = A_{cont}[\mathbf{n} : \dot{\mathbf{e}}] \tag{3.1}$$

A_{cont} being a scalar parameter, depending on the particular material model; for the three models discussed in the paper, we will present an explicit expression for A_{cont}. Note that if the limit function F involves an explicit dependence on the consistency parameter (see Table 1), equation 3.1 can be obtained directly from the condition $F = 0$; if F does not involve $\dot{\gamma}$ explicitly, we use the condition $\dot{F} = 0$.

3.2 Continuous elasto-plastic tangent tensor

To compute the elasto-plastic tangent tensor for the continuous model we start from the rate form of the linear elastic relation between $\mathbf{s}$ and $\mathbf{e}$ (equation 2.12) and the evolution equation for the back stress (equation 2.22), which are rewritten in matrix form as:

$$\begin{bmatrix} \mathbf{I} & 0 & 2G\mathbf{n} \\ 0 & \mathbf{I} & -[H_{kin}\mathbf{n} - H_{nl}\boldsymbol{\alpha}] \end{bmatrix} \begin{Bmatrix} \dot{\mathbf{s}} \\ \dot{\boldsymbol{\alpha}} \\ \dot{\gamma} \end{Bmatrix} = \begin{Bmatrix} 2G\dot{\mathbf{e}} \\ 0 \end{Bmatrix}$$

$\mathbf{I}$ being the fourth order identity tensor. Recalling equation 3.1, we obtain:

$$\begin{bmatrix} \mathbf{I} & 0 \\ 0 & \mathbf{I} \end{bmatrix} \begin{Bmatrix} \dot{\mathbf{s}} \\ \dot{\boldsymbol{\alpha}} \end{Bmatrix} = \begin{Bmatrix} 2G\left[\mathbf{I} - A_{cont}\left(\mathbf{n} \otimes \mathbf{n}\right)\right]\dot{\mathbf{e}} \\ A_{cont}\left[H_{kin}\left(\mathbf{n} \otimes \mathbf{n}\right) - H_{nl}\left(\boldsymbol{\alpha} \otimes \mathbf{n}\right)\right]\dot{\mathbf{e}} \end{Bmatrix} \tag{3.2}$$

Expansion of the first row yields:

$$\dot{\mathbf{s}} = 2G\left[\mathbf{I} - A_{cont}(\mathbf{n} \otimes \mathbf{n})\right]\dot{\mathbf{e}}$$

which can be transformed to obtain a rate relation between the total stress $\boldsymbol{\sigma}$ and the total strain $\boldsymbol{\epsilon}$:

$$\dot{\boldsymbol{\sigma}} = \mathbf{D}_{cont}\dot{\boldsymbol{\epsilon}}$$

where:

$$\mathbf{D}_{cont} = \{K\,(\mathbf{1}\otimes\mathbf{1}) + 2G\,[\mathbf{I}_{dev} - A_{cont}(\mathbf{n}\otimes\mathbf{n})]\} \tag{3.3}$$

$\mathbf{I}_{dev}$ being a rank four tensor defined as:

$$\mathbf{I}_{dev} = \mathbf{I} - \frac{1}{3}(\mathbf{1}\otimes\mathbf{1})$$

In equation 3.3, $\mathbf{D}_{cont}$ is the elasto-plastic tangent tensor, consistent with the continuous model discussed in Section 2. Note that the symmetry of the tensor is not destroyed by a non-associative kinematic hardening rule, since the two sets of equations in 3.2 are decoupled.

4 DISCRETE TIME MODEL AND ALGORITHMIC IMPLEMENTATION

We now present the discrete time counterpart for the analysis performed in Sections 2 and 3, paying particular attention to an implementation of the model within a radial return map algorithm. The form of the elasto-plastic tangent tensor consistent with the discrete model is also addressed.

4.1 Discrete equations and integration algorithm

From a computational standpoint we treat the non-linear behavior of a material as a *strain driven* problem, since in a finite element implementation the stress history is computed from the strain history by an integration technique, such as a return mapping algorithm. Accordingly, we introduce a discrete counterpart of the equations presented in Section 2 and review the integration algorithm.

Let $[0,T] \subset \mathcal{R}$ be the time interval of interest and consider two time values within it, say t_n and $t_{n+1} > t_n$, such that t_{n+1} is the first time value

of interest after t_n. To minimize the appearance of subscripts (to make the equations more readable), we introduce the convention:

$$\mathbf{a}_n = \mathbf{a}(t_n) \ , \quad \mathbf{a} = \mathbf{a}(t_{n+1})$$

where $\mathbf{a}$ is any generic quantity. Accordingly, in the discrete time setting the subscript n indicates a quantity evaluated at time t_n, while no subscript indicates a quantity evaluated at time t_{n+1}.

We assume that the solution is known at time t_n and given by the state:

$$\{\mathbf{s}_n, \mathbf{e}_n, \mathbf{e}^p_n, \bar{e}^p_n, \boldsymbol{\alpha}_n\}$$

We wish to compute the solution at time t_{n+1}, given the strain $\mathbf{e}$. Using a backward Euler integration formula for the plastic strain, the accumulative plastic strain flow and the back stress rules (equations 2.16, 2.21 and 2.22), we obtain:

$$\mathbf{e}^p = \mathbf{e}^p_n + \lambda\, \mathbf{n} \tag{4.1}$$

$$\bar{e}^p = \bar{e}^p_n + \lambda \tag{4.2}$$

$$R^\lambda \boldsymbol{\alpha} = \boldsymbol{\alpha}_n + H_{kin}\lambda \mathbf{n} \quad or \quad \boldsymbol{\alpha} = T^\lambda \boldsymbol{\alpha}_n + H_{kin} T^\lambda \lambda \mathbf{n} \tag{4.3}$$

where:

$$\lambda = \int_{t_n}^{t_{n+1}} \dot{\gamma} dt$$

is the discrete consistency parameter and:

$$R^\lambda = 1 + H_{nl}\lambda \quad , \quad T^\lambda = \frac{1}{1 + H_{nl}\lambda}$$

From now on, the presence of a superscript λ indicates a dependence on the consistency parameter. Substitution of equation 4.1 into equation 2.12 yields:

$$\mathbf{s} = 2G\ [\mathbf{e} - \mathbf{e}^p_n] - 2G\, \lambda\, \mathbf{n} \tag{4.4}$$

and subtraction of equation 4.3 gives:

$$\boldsymbol{\Sigma} = \mathbf{s} - \boldsymbol{\alpha} = 2G\,[\mathbf{e} - \mathbf{e}^p_n] - T^\lambda \boldsymbol{\alpha}_n - U^\lambda \mathbf{n} \tag{4.5}$$

where:

$$U^{\lambda} = \left[2G + H_{kin}T^{\lambda}\right]\lambda$$

In the above, λ is an unknown quantity and is computed by means of an integration algorithm, such as a return mapping procedure. Initially suggested by Maenchen and Sack [31] and Wilkins [52], the return mapping algorithm provides an efficient and robust integration scheme, based on a discrete enforcement of the limit equation. It belongs to the family of elastic-predictor plastic-corrector algorithms and, hence, is a two part algorithm. In the first part, a purely elastic *trial state* is computed; in the second, if the trial state violates the material model constitutive equation, a correction is computed using the trial state as initial condition and applied such that the final state is fully consistent with the discrete model. The algorithm has been widely studied [38, 45, 44] as has its stability [23, 43]. Recalling that the incremental elasto-plastic initial value problem formulated as a constrained convex minimization problem is equivalent to the classical *maximum plastic dissipation* postulate, the return mapping algorithm can be shown to be equivalent to a closest point projection of the trial state onto the limit surface $F = 0$. Additional discussion of the algorithm and its theoretical implication can be found in Reference [44].

We shall now discuss the two steps of the algorithm in more details.

- *Trial state*: we assume that in the interval $[t_n, t_{n+1}]$ no plastic deformation occurs (i.e. $\mathbf{e}^p = \mathbf{e}^p_n$, which implies: $\lambda = 0$, $\boldsymbol{\alpha} = \boldsymbol{\alpha}_n$). As a result, we have as trial values:

$$\begin{aligned}
\lambda^{TR} &= 0 \\
\mathbf{e}^{p,TR} &= \mathbf{e}^p_n \\
\bar{e}^{p,TR} &= \bar{e}^p_n \\
\boldsymbol{\alpha}^{TR} &= \boldsymbol{\alpha}_n \\
\mathbf{s}^{TR} &= 2G\left[\mathbf{e} - \mathbf{e}^p_n\right] \\
\boldsymbol{\Sigma}^{TR} &= \mathbf{s}^{TR} - \boldsymbol{\alpha}^{TR} = \mathbf{s}^{TR} - \boldsymbol{\alpha}_n
\end{aligned}$$

  If the elastic trial state is admissible, i.e. it does not violate the limit equation F, then it represents the new solution at t_{n+1} and the second part of the algorithm is skipped. If the elastic trial state is not admissible, a correction has to be performed.

- *Plastic correction*: enforcing the satisfaction of the limit equation, the consistency parameter λ may be computed, as shown for various material model in Sections 5, 6 and 7. Equations 4.1, 4.2, 4.3_2, 4.4 and 4.5 can be now rewritten in terms of the trial state and λ:

$$\begin{aligned} \mathbf{e}^p &= \mathbf{e}^{p,TR} + \lambda \mathbf{n} \\ \bar{e}^p &= \bar{e}^{p,TR} \\ \boldsymbol{\alpha} &= T^\lambda \boldsymbol{\alpha}^{TR} + H_{kin} T^\lambda \lambda \mathbf{n} \\ \mathbf{s} &= \mathbf{s}^{TR} - 2G\,\lambda\,\mathbf{n} \\ \boldsymbol{\Sigma} &= \mathbf{s}^{TR} - T^\lambda \boldsymbol{\alpha}^{TR} - U^\lambda \mathbf{n} \end{aligned}$$

  which allow us to compute and update the solution.

For all the models discussed in the paper, and more generally for all J2 materials with an associative flow rule and a non-linear kinematic hardening, we now show how the closest point projection of the trial state onto the limit surface $F = 0$ reduces to a radial return projection. Consequently, the consistency parameter λ may be computed by solving only a scalar equation. First we note that the relative stress $\boldsymbol{\Sigma}$ can be decomposed as:

$$\boldsymbol{\Sigma} = \boldsymbol{\Sigma}_A^\lambda - U^\lambda \mathbf{n} \tag{4.6}$$

where:

$$\boldsymbol{\Sigma}_A^\lambda = \left[\mathbf{s}^{TR} - T^\lambda \boldsymbol{\alpha}^{TR}\right]$$

Secondly, we observe that $\boldsymbol{\Sigma}$ is in the $\mathbf{n}$-direction, i.e. $\boldsymbol{\Sigma} = \|\boldsymbol{\Sigma}\|\,\mathbf{n}$, since:

$$\begin{aligned} \mathbf{n} &= \frac{\partial f}{\partial \boldsymbol{\sigma}} = \frac{\partial f}{\partial \boldsymbol{\Sigma}} \frac{\partial \boldsymbol{\Sigma}}{\partial \boldsymbol{\sigma}} = \frac{\partial f}{\partial \boldsymbol{\Sigma}} \mathbf{I}_{dev} \\ &= \frac{\partial \|\boldsymbol{\Sigma}\|}{\partial \boldsymbol{\Sigma}} \mathbf{I}_{dev} = \frac{\boldsymbol{\Sigma}}{\|\boldsymbol{\Sigma}\|} \mathbf{I}_{dev} = \frac{\boldsymbol{\Sigma}}{\|\boldsymbol{\Sigma}\|} \end{aligned}$$

Hence, from equation 4.6, we may conclude that $\boldsymbol{\Sigma}_A^\lambda$ must be also in the direction of $\mathbf{n}$, i.e. $\boldsymbol{\Sigma}_A^\lambda = \|\boldsymbol{\Sigma}_A^\lambda\|\,\mathbf{n}$. Consequently, a scalar relation between the norms of $\boldsymbol{\Sigma}$ and $\boldsymbol{\Sigma}_A^\lambda$ may be generated:

$$\|\boldsymbol{\Sigma}\| = \|\boldsymbol{\Sigma}_A^\lambda\| - U^\lambda \tag{4.7}$$

This situation differs from the standard return mapping algorithm (i.e., the one obtained for classical plasticity) for which the direction $\mathbf{n}$ is determined by $\boldsymbol{\Sigma}^{TR}$, which is a quantity independent from λ. In the more general setting here discussed, $\mathbf{n}$ is also function of λ; this makes the return algorithm slightly more complicated, but still a radial return may be performed.

4.2 Discrete constitutive equation for the plastic strain

The general form of the discrete constitutive equation for the plastic strain has already been introduced in equation 4.1, obtained from the corresponding continuous constitutive equation through integration. The missing ingredient is the value of the discrete parameter λ, which should be computed by requiring the satisfaction of the material model in a discrete setting.

We assume that from the discrete limit equation, an analogous discrete counterpart of equation 3.1 can be obtained:

$$d\lambda = A_{discr}[\mathbf{n} : d\mathbf{e}]$$

A_{discr} being a scalar quantity depending on the material model. Starting from Section 5, we discuss how λ and A_{discr} can be computed for the material models of Table 1.

4.3 Discrete elasto-plastic tangent tensor

We address a simple and efficient approach for constructing the elasto-plastic tangent tensor, consistent with the discrete model. The use of a consistent tangent tensor preserves the quadratic convergence of a Newton method, which we adopt in Section 8 for the incremental solution of a finite element scheme. Following the same approach of Section 3.2 but within a discrete time setting, we start from the linear elastic relation between $\mathbf{s}$ and $\mathbf{e}$ and from the discrete evolution equation for $\boldsymbol{\alpha}$:

$$\begin{aligned} \mathbf{s} &= 2G\,[\mathbf{e} - \mathbf{e}_n^p] - 2G\lambda\mathbf{n} \\ R^\lambda\boldsymbol{\alpha} &= \boldsymbol{\alpha}_n + H_{kin}\lambda\mathbf{n} \end{aligned}$$

and by linearization we obtain:

$$d\mathbf{s} = 2G d\mathbf{e} - 2G d\lambda\ \mathbf{n} - 2G\lambda\ d\mathbf{n} \tag{4.8}$$

$$R^{\lambda} d\boldsymbol{\alpha} + H_{nl} d\lambda \, \boldsymbol{\alpha} = H_{kin} d\lambda \, \mathbf{n} + H_{kin} \lambda \, d\mathbf{n} \tag{4.9}$$

Keeping in mind that:

$$\mathbf{n} = \frac{\boldsymbol{\Sigma}}{\|\boldsymbol{\Sigma}\|} = \frac{\boldsymbol{\Sigma}}{\left[(\boldsymbol{\Sigma} : \boldsymbol{\Sigma})^{\frac{1}{2}}\right]}$$

we can compute its variation:

$$d\mathbf{n} = \frac{1}{\|\boldsymbol{\Sigma}\|} \left[\mathbf{I} - (\mathbf{n} \otimes \mathbf{n})\right] d\boldsymbol{\Sigma} = \frac{\mathbf{N}}{\|\boldsymbol{\Sigma}\|} d\boldsymbol{\Sigma}$$

where the fourth order tensor $\mathbf{N}$ is the orthogonal projection operator on the plane with unit normal $\mathbf{n}$, such that:

$$\mathbf{N}\mathbf{n} = 0 \quad and \quad \mathbf{N}\mathbf{N} = \mathbf{N}$$

Accordingly, equations 4.8 and 4.9 can be recast in matrix form in terms of the unknown $d\mathbf{s}$, $d\boldsymbol{\alpha}$, $d\lambda$:

$$\begin{bmatrix} \mathbf{I} + a\mathbf{N} & -a\mathbf{N} & 2G\mathbf{n} \\ -b\mathbf{N} & R^{\lambda}\mathbf{I} + b\mathbf{N} & -H_{kin}\mathbf{n} + H_{nl}\boldsymbol{\alpha} \end{bmatrix} \begin{Bmatrix} d\mathbf{s} \\ d\boldsymbol{\alpha} \\ d\lambda \end{Bmatrix} = \begin{Bmatrix} 2G d\mathbf{e} \\ 0 \end{Bmatrix}$$

where:

$$a = \frac{2G\lambda}{\|\boldsymbol{\Sigma}\|} \quad , \quad b = \frac{H_{kin}\lambda}{\|\boldsymbol{\Sigma}\|}$$

Since $d\lambda = A_{discr} \, [\mathbf{n} : d\mathbf{e}]$, the previous system of equations simplifies to:

$$\begin{bmatrix} \mathbf{I} + a\mathbf{N} & -a\mathbf{N} \\ -b\mathbf{N} & R^{\lambda}\mathbf{I} + b\mathbf{N} \end{bmatrix} \begin{Bmatrix} d\mathbf{s} \\ d\boldsymbol{\alpha} \end{Bmatrix} = \begin{Bmatrix} 2G\left[(1 + A_{discr})\mathbf{I} - A_{discr}\mathbf{N}\right] d\mathbf{e} \\ A_{discr}\left[H_{kin}(\mathbf{n} \otimes \mathbf{n}) - H_{nl}(\boldsymbol{\alpha} \otimes \mathbf{n})\right] d\mathbf{e} \end{Bmatrix}$$

Inverting the coefficient matrix, we may solve for $d\mathbf{s}$ and $d\boldsymbol{\alpha}$:

$$\begin{Bmatrix} d\mathbf{s} \\ d\boldsymbol{\alpha} \end{Bmatrix} = \begin{bmatrix} \mathbf{I} + \alpha_1\mathbf{N} & -\alpha_3\mathbf{N} \\ -\alpha_2\mathbf{N} & \dfrac{1}{R^{\lambda}}\mathbf{I} + \alpha_2\mathbf{N} \end{bmatrix} \begin{Bmatrix} 2G\left[(1 + A_{discr})\mathbf{I} - A_{discr}\mathbf{N}\right] d\mathbf{e} \\ A_{discr}\left[H_{kin}(\mathbf{n} \otimes \mathbf{n}) - H_{nl}(\boldsymbol{\alpha} \otimes \mathbf{n})\right] d\mathbf{e} \end{Bmatrix}$$

where:

$$\begin{aligned} \alpha_1 &= -\frac{aR^\lambda}{b+R^\lambda+aR^\lambda} \\ \alpha_2 &= -\frac{b}{b+R^\lambda+aR^\lambda} \\ \alpha_3 &= -\frac{a}{b+R^\lambda+aR^\lambda} = \frac{\alpha_1}{R^\lambda} \end{aligned}$$

Expanding the first row and performing some manipulations, we yield the relation:

$$d\mathbf{s} = \{2G(1-C)\mathbf{I} + [2G(C-A_{discr}) + B(\mathbf{n}:\boldsymbol{\alpha})](\mathbf{n}\otimes\mathbf{n}) - B(\boldsymbol{\alpha}\otimes\mathbf{n})\}\, d\mathbf{e}$$

where:

$$B = A_{discr} T^\lambda C H_{nl} \tag{4.10}$$

$$C = \frac{2G\lambda}{\|\boldsymbol{\Sigma}_A^\lambda\|} = -\alpha_2 \tag{4.11}$$

Finally, we can get the incremental relation between the total stress $\boldsymbol{\sigma}$ and the total strain $\boldsymbol{\epsilon}$, consistent with the discrete model presented in Section 4.1:

$$d\boldsymbol{\sigma} = \mathbf{D}_{discr}\, d\boldsymbol{\epsilon}$$

where the algorithmic elasto-plastic tangent tensor is given by:

$$\begin{aligned} \mathbf{D}_{discr} &= K(\mathbf{1}\otimes\mathbf{1}) + 2G(1-C)\mathbf{I}_{dev} \\ &\quad + [2G(C-A_{discr}) + B(\mathbf{n}:\boldsymbol{\alpha})](\mathbf{n}\otimes\mathbf{n}) - B(\boldsymbol{\alpha}\otimes\mathbf{n}) \end{aligned} \tag{4.12}$$

We recall that the coefficients B and C are defined in equations 4.10 and 4.11, respectively, while A_{discr} comes from the linearized limit equation for the specific material model.

We conclude pointing out that a straightforward approach for the construction of the consistent elasto-plastic tangent tensor has been shown for any material model that fits in the framework discussed in Section 2; however, this tensor is non-symmetric, in the presence of a non-associative kinematic hardening mechanism, such as the one proposed by Armstrong and Frederick in Reference [1].

5 CLASSICAL PLASTICITY MODEL

We now specializes the discussion of Sections 3 and 4 to a simple and well established classical plasticity model. The model is obtained by setting the limit function F to coincide with the yield function f and choosing a linear evolution equation for the kinematic hardening mechanism:

$$F = f = \|\boldsymbol{\Sigma}\| - R$$

$$\dot{\boldsymbol{\alpha}} = H_{kin}\dot{\gamma}\mathbf{n} \quad , \quad H_{nl} = 0$$

As a result, we have:

$$R^{\lambda} = 1 \quad , \quad T^{\lambda} = 1 \quad , \quad U^{\lambda} = [2G + H_{kin}]\,\lambda$$

5.1 Continuous model

Since the limit function F does not depend explicitly on $\dot{\gamma}$, as discussed in Section 3.1, we use the condition $\dot{F} = 0$ to compute an expression for the consistency parameter. By the chain rule we have:

$$\begin{aligned} \dot{F} &= \frac{\partial F}{\partial \boldsymbol{\Sigma}} : \dot{\boldsymbol{\Sigma}} + \frac{\partial F}{\partial \bar{e}^p}\dot{\bar{e}}^p \\ &= \frac{\partial f}{\partial \boldsymbol{\Sigma}} : \dot{\boldsymbol{\Sigma}} + \frac{\partial f}{\partial \bar{e}^p}\dot{\bar{e}}^p \\ &= \mathbf{n} : \dot{\mathbf{s}} - \mathbf{n} : \dot{\boldsymbol{\alpha}} - H_{iso}\dot{\bar{e}}^p = 0 \end{aligned}$$

where we noted that:

$$\frac{\partial f}{\partial \bar{e}^p} = -\frac{\partial \sigma_y}{\partial \bar{e}^p} = -H_{iso}$$

Substitution of equation 2.21 and use of the rate of equation 2.12 yield:

$$\dot{F} = 2G[\mathbf{n} : \dot{\mathbf{e}}] - [2G + H_{iso} + H_{kin}]\,\dot{\gamma} = 0$$

which can be solved in terms of $\dot{\gamma}$:

$$\dot{\gamma} = A^{CP}_{cont}[\mathbf{n} : \dot{\mathbf{e}}]$$

where:

$$A^{CP}_{cont} = \frac{G}{G_1}$$

with:

$$2G_1 = 2G + H_{iso} + H_{kin}$$

Once the scalar quantity A^{CP}_{cont} is computed, a mere substitution into equation 3.3 returns the continuous elasto-plastic tangent tensor relative to this specific model:

$$\mathbf{D}^{CP}_{cont} = \left\{ K\,(\mathbf{1}\otimes\mathbf{1}) + 2G\,\left[\mathbf{I}_{dev} - A^{CP}_{cont}(\mathbf{n}\otimes\mathbf{n})\right]\right\}$$

5.2 Discrete algorithmic model

As a result of $H_{nl} = 0$, the following simplifications occur:

$$\begin{aligned}
\boldsymbol{\alpha} &= \boldsymbol{\alpha}^{TR} + H_{kin}\lambda\mathbf{n} \\
\boldsymbol{\Sigma}^{\lambda}_{A} &= \boldsymbol{\Sigma}^{TR} = \mathbf{s}^{TR} - \boldsymbol{\alpha}^{TR} \\
\boldsymbol{\Sigma} &= \boldsymbol{\Sigma}^{TR} - [2G + H_{kin}]\,\lambda\mathbf{n}
\end{aligned}$$

Looking at the last relation, we may conclude that now $\boldsymbol{\Sigma}^{TR}$ and $\boldsymbol{\Sigma}$ are parallel and consequently a scalar relation between their norms may be derived:

$$\|\boldsymbol{\Sigma}\| = \|\boldsymbol{\Sigma}^{TR}\| - [2G + H_{kin}]\,\lambda$$

Recalling equation 2.20, the radius of the yield surface σ_y may be expressed as:

$$\begin{aligned}
\sigma_y &= \sigma_{y,0} + H_{iso}\bar{e}^p \\
&= \sigma_{y,0} + H_{iso}(\bar{e}^p_n + \lambda) \\
&= \sigma_{y,n} + H_{iso}\,\lambda
\end{aligned}$$

such that the discrete form of the limit equation can be enforced:

$$F = f = \left[\|\boldsymbol{\Sigma}^{TR}\| - (2G + H_{kin})\,\lambda\right] - (\sigma_{y,n} + H_{iso}\lambda) = 0$$

and solved for λ:

$$\lambda^{CP} = \frac{\|\boldsymbol{\Sigma}^{TR}\| - \sigma_{y,n}}{2G_1}$$

From the linearization of the discrete limit equation, we get:

$$\begin{aligned} dF &= \frac{\partial F}{\partial \boldsymbol{\Sigma}} : d\boldsymbol{\Sigma} + \frac{\partial F}{\partial \bar{e}^p} d\bar{e}^p \\ &= \frac{\partial f}{\partial \boldsymbol{\Sigma}} : d\boldsymbol{\Sigma} + \frac{\partial f}{\partial \bar{e}^p} d\bar{e}^p \\ &= \mathbf{n} : d\mathbf{s} - \mathbf{n} : d\boldsymbol{\alpha} - H_{iso} d\bar{e}^p = 0 \end{aligned}$$

and using equations 4.8 and 4.9, with $H_{nl} = 0$ and $R^\lambda = 1$, dF reduces to:

$$dF = 2G[\mathbf{n} : d\mathbf{e}] - [2G + H_{iso} + H_{kin}]d\lambda = 0$$

This last relation can be solved for $d\lambda$, obtaining:

$$d\lambda = A^{CP}_{discr}[\mathbf{n} : d\mathbf{e}]$$

where:

$$A^{CP}_{discr} = \frac{G}{G_1} = A^{CP}_{cont}$$

Finally, from equation 4.12, noting that $B = 0$, we can write the elasto-plastic tangent tensor consistent with the discrete form of the classical plasticity model:

$$\mathbf{D}^{CP}_{discr} = \left\{ K\,(\mathbf{1} \otimes \mathbf{1}) + 2G\,\left(1 - C^{CP}\right)\,\mathbf{I}_{dev} + \left[2G\,\left(C^{CP} - A^{CP}_{discr}\right)\right](\mathbf{n} \otimes \mathbf{n}) \right\}$$

where:

$$C^{CP} = \frac{2G\lambda}{\|\boldsymbol{\Sigma}^{TR}\|}$$

Note that the continuous form of the tangent tensor coincides with the case $C^{CP} = 0$, which is also the values attained as the load step reduces to zero.

5.3 Remarks on the classical plasticity model

Classical plasticity is a well known and widely used model, especially in the simple form discussed here, relative to a J2 material.

The model is based on linear evolutionary rules for both the plastic strain and the kinematic hardening; as a result, only piece-wise linear stress strain relation can be obtained. In figures 1 and 2 two typical $\boldsymbol{\sigma} - \epsilon$ curves are represented, relative to a uni-axial tension problem. Note that if the model

is unloaded from the plastic range and reloaded before the occurrence of plasticity in the reverse direction, it renews plasticity at the same stress where unloading began. This behavior is in contrast with experimental evidence for many materials, such as aluminum and copper, which renew plasticity at a lower value of the stress under this type of unloading-reloading path, as discussed in References [40, 42, 27]. Typical responses of the model under cyclic loading conditions are reported in figures 3 and 4.

On the other hand, from the previous discussion, it is clear that the model has a simple and straightforward algorithmic implementation; in fact, the condition $F = 0$ yields a linear equation in λ and the consistent elasto-plastic tangent tensor is symmetric, for both the continuous and the discrete model.

We may conclude noting that, despite its simple algorithmic implementation, the classical plasticity is unable to closely simulate the behavior of real materials; hence, some improvements are needed.

6 NON-LINEAR KINEMATIC HARDENING MODEL

For the NLK model the constitutive equations specialize as:

$$F = f = \|\boldsymbol{\Sigma}\| - \sigma_y$$

$$\dot{\boldsymbol{\alpha}} = H_{kin}\dot{\gamma}\mathbf{n} + H_{nl}\dot{\gamma}\boldsymbol{\alpha}$$

where the first equation clearly states that the limit and the yield functions coincide, while the second equation is the non-linear evolutionary equation for the kinematic hardening, initially proposed by Armstrong and Frederick [1]. In the last decade, the model has been extensively studied by several authors; in particular Chaboche et al. showed that the model performs well in simulating the behavior of some real materials [4, 5, 7, 8, 6, 9, 26].

6.1 Continuous model

Recalling the discussion of Sections 3.1 and 5.1, the consistency condition yields:

$$\dot{F} = 2G[\mathbf{n} : \dot{\mathbf{e}}] - \{2G + H_{iso} + H_{kin} - H_{nl}[\mathbf{n} : \boldsymbol{\alpha}]\}\dot{\gamma} = 0$$

which can be solved in terms of $\dot{\gamma}$, obtaining:

$$\dot{\gamma} = A_{cont}^{NLK}[\mathbf{n} : \dot{\mathbf{e}}]$$

where:

$$A_{cont}^{NLK} = \frac{2G}{2G_1 - H_{nl}[\mathbf{n} : \boldsymbol{\alpha}]}$$

Hence, a direct application of equation 3.3 returns the consistent continuous elasto-plastic tangent tensor:

$$\mathbf{D}_{cont}^{NLK} = \left\{ K\,(\mathbf{1} \otimes \mathbf{1}) + 2G\,\left[\mathbf{I}_{dev} - A_{cont}^{NLK}(\mathbf{n} \otimes \mathbf{n})\right] \right\}$$

6.2 Discrete algorithmic model

As discussed in Section 4.1, a radial return mapping algorithm may be performed also for the NLK model. In fact, recalling equation 4.7, the discrete limit equation can be written as:

$$\|\boldsymbol{\Sigma}_A^\lambda\| - U^\lambda - \sigma_y = 0$$

Noting that:

$$\begin{aligned}
\|\boldsymbol{\Sigma}_A^\lambda\| &= \left[(\boldsymbol{\Sigma}_A^\lambda : \boldsymbol{\Sigma}_A^\lambda)\right]^{\frac{1}{2}} \\
&= \left[\left(\mathbf{s}^{TR} - T^\lambda \boldsymbol{\alpha}^{TR}\right) : \left(\mathbf{s}^{TR} - T^\lambda \boldsymbol{\alpha}^{TR}\right)\right]^{\frac{1}{2}} \\
&= \left[(\mathbf{s}^{TR} : \mathbf{s}^{TR}) - 2T^\lambda(\boldsymbol{\alpha}^{TR} : \mathbf{s}^{TR}) + (T^\lambda)^2(\boldsymbol{\alpha}^{TR} : \boldsymbol{\alpha}^{TR})\right]^{\frac{1}{2}} \\
&= \left[S_{ss} - 2S_{s\alpha}T^\lambda + S_{\alpha\alpha}(T^\lambda)^2\right]^{\frac{1}{2}}
\end{aligned}$$

where:

$$\begin{aligned}
S_{ss} &= (\mathbf{s}^{TR} : \mathbf{s}^{TR}) \\
S_{s\alpha} &= (\mathbf{s}^{TR} : \boldsymbol{\alpha}^{TR}) \\
S_{\alpha\alpha} &= (\boldsymbol{\alpha}^{TR} : \boldsymbol{\alpha}^{TR})
\end{aligned}$$

the limit equation becomes:

$$S_{ss}(R^\lambda)^2 - 2S_{s\alpha}R^\lambda + S_{\alpha\alpha} - \left[2G\lambda R^\lambda + H_{kin}\lambda + R^\lambda\sigma_{y,n} + H_{iso}\lambda R^\lambda\right]^2 = 0$$

Reordering for λ, a quartic equation is obtained:

$$g(\lambda) = C_1\lambda^4 + C_2\lambda^3 + C_3\lambda^2 + C_4\lambda + C_5 = 0$$

where:

$$\begin{aligned}
C_1 &= 4{H_{nl}}^2 G_0^2 \\
C_2 &= 4{H_{nl}}^2 G_0 \sigma_{y,n} + 8 G_0 G_1 H_{nl} \\
C_3 &= {H_{nl}}^2 \left[(\sigma_{y,n})^2 - S_{ss}\right] + 4G_1^2 + 4H_{nl}\sigma_{y,n}\left[G_0 + G_1\right] \\
C_4 &= 2H_{nl}\left[(\sigma_{y,n})^2 + S_{s\alpha} - S_{ss}\right] + 4\sigma_{y,n}G_1 \\
C_5 &= (\sigma_{y,n})^2 - S_{\alpha\alpha} + 2S_{s\alpha} - S_{ss}
\end{aligned}$$

with:

$$2G_0 = 2G + H_{iso}$$

The solution of this equation, i.e. the search of the minimum positive root, is not an easy task, due to the order of the polynomial and to the dependence of the coefficients on the trial state. An iterative algorithm of the Newton type may be easily implemented:

$$\begin{aligned}
\lambda^{i+1} &= \lambda^i + \Delta\lambda^i \\
\Delta\lambda^i &= -\frac{g\left(\lambda^i\right)}{g'\left(\lambda^i\right)}
\end{aligned}$$

where: the superscript i refers to the i-th iteration, the superscript $'$ indicates first derivative; and where a starting value of $\lambda^0 = 0$ may be adopted. Unfortunately, this approach does not guarantee the convergence to an existing or positive root; in fact:

$$\begin{aligned}
\Delta\lambda(0) &= -\frac{g(0)}{g'(0)} = -\frac{C_5}{C_4} \\
&= \frac{\boldsymbol{\Sigma}^{TR} : \boldsymbol{\Sigma}^{TR} - (\sigma_{y,n})^2}{2H_{nl}\left[\boldsymbol{\Sigma}^{TR} : \boldsymbol{\Sigma}^{TR} - (\sigma_{y,n})^2\right] + 2H_{nl}(\boldsymbol{\Sigma}^{TR} : \boldsymbol{\alpha}^{TR}) - 4\sigma_{y,n}G_1}
\end{aligned}$$

and the sign of $\Delta\lambda$ at zero depends on the sign of the denominator, which clearly depends on the trial state and on the previous solution. Consequently, it may happen that $\Delta\lambda(0) < 0$ and the Newton algorithm returns a negative

value for λ. Attempts of starting the Newton iteration algorithm with different values of λ (such as $\lambda^0 = \lambda_n$) have been explored but generate the same pathology. Once the Newton algorithm has failed, the only robust approach is to perform a synthetic division of the quartic polynomial and compute in closed form the roots of the resulting cubic [41]; the smallest positive root computed root so founded should be filtered through a Newton algorithm, since the synthetic division is sensitive to roundoff.

Recalling equations 4.8 and 4.9 and the discussion of Section 5.2, we have:

$$\begin{aligned} \mathbf{n} : d\mathbf{s} &= 2G[\mathbf{n} : d\mathbf{e}] - 2Gd\lambda \\ \mathbf{n} : d\boldsymbol{\alpha} &= T^\lambda H_{kin} d\lambda - T^\lambda H_{nl}[\mathbf{n} : \boldsymbol{\alpha}] d\lambda \end{aligned}$$

such that the discrete consistency condition can be formulated as:

$$dF = 2G[\mathbf{n} : d\mathbf{e}] - \left\{2G + H_{iso} + T^\lambda H_{kin} - T^\lambda H_{nl}[\mathbf{n} : \boldsymbol{\alpha}]\right\} d\lambda = 0$$

Solving for $d\lambda$, we obtain:

$$d\lambda = A^{NLK}_{discr}[\mathbf{n} : d\mathbf{e}]$$

where:

$$A^{NLK}_{discr} = \frac{2G}{2G_0 + T^\lambda H_{kin} - T^\lambda H_{nl}[\mathbf{n} : \boldsymbol{\alpha}]}$$

Recalling the discussion of Section 4.3, the elasto-plastic tangent tensor consistent with the discrete model can be computed:

$$\begin{aligned} \mathbf{D}^{NLK}_{discr} &= K\,(\mathbf{1} \otimes \mathbf{1}) + 2G\,(1 - C)\,\mathbf{I}_{dev} \\ &\quad + \left[2G\,(C - A^{NLK}_{discr}) + B(\mathbf{n} : \boldsymbol{\alpha})\right](\mathbf{n} \otimes \mathbf{n}) - B(\boldsymbol{\alpha} \otimes \mathbf{n}) \end{aligned}$$

where:

$$\begin{aligned} B &= A^{NLK}_{discr} T^\lambda C H_{nl} \\ C &= \frac{2G\lambda}{\|\boldsymbol{\Sigma}^\lambda_A\|} \end{aligned}$$

6.3 Remarks on the model

The NLK model represents an improvement with respect to the CP model. In fact, as qualitatively shown in figure 5 for the case of uni-axial tension, the model has the property of smoothly reaching an asymptotic stress value. Moreover, it retains the capacity of smooth transition between elastic and plastic behavior also under cyclic loading condition, as qualitatively shown in figure 6. However, the asymptote can be only horizontal and, if unloaded from the plastic range and reloaded before the occurrence of reverse plasticity, the model renews plasticity exactly at the same stress where unloading began (see figure 5). This behavior is in contrast with some experimental results, such as the ones presented in Reference [27].

The NLK model has been frequently used by several authors to simulate the behavior of real materials. In particular, Chaboche has presented interesting applications as well as extensions of the model to include strain range memory, visco-plastic recovery properties, ratcheting effects [4, 5, 7, 8, 6, 9, 26]. This clearly makes the NLK widely used in the modelling of metals under cyclic loading paths and a high degree of accuracy in the simulation may be achieved.

It is however clear from the previous discussion that difficulties arise to implement the model in a return mapping framework and they are all directly related to the form of the non-linear kinematic hardening rule. In fact, the discrete consistency condition yields a quartic equation, whose coefficients are function of the trial state and the previous solution, which makes difficult the search of the minimum positive root. A robust approach based on a combination of Newton's algorithm and synthetic division is presented, which is computationally quite expensive. Moreover, the elasto-plastic tangent tensor consistent with the discrete model is non-symmetric and, as a result, an appropriate solver must be used, plus the required memory storage is doubled.

7 GENERALIZED PLASTICITY MODEL

A simple model for generalized plasticity was introduced by Lubliner and the authors in References [30] and [3]. Referring to the notation of Reference [3],

the limit equation and the evolutionary equation for $\boldsymbol{\alpha}$ are respectively:

$$\begin{aligned} F &= h(f)\,[\mathbf{n} : \dot{\boldsymbol{\sigma}}] - \dot{\gamma} \\ \dot{\boldsymbol{\alpha}} &= H_{kin}\dot{\gamma}\mathbf{n} \quad , \quad H_{nl} = 0 \end{aligned}$$

where:

$$h(f) = \frac{f}{\delta(\beta - f) + H\beta} \quad , \quad \mathbf{n} = \frac{\partial f}{\partial \boldsymbol{\sigma}}$$

with β and δ two positive constants with dimensions of stress and $H = H_{iso} + H_{kin}$. In particular β is a scalar measure of the distance between the asymptotic and the current radius of the yield function σ_y, while δ measures the speed of the model in approaching the asymptotic behavior (see figure 7 and 8).

Recalling the discussion in Section 2, we have:

$$\begin{aligned} \mathbf{n} : \dot{\boldsymbol{\sigma}} &= \mathbf{n} : \dot{\mathbf{s}} = \mathbf{n} : \dot{\boldsymbol{\Sigma}} + \mathbf{n} : \dot{\boldsymbol{\alpha}} = \mathbf{n} : \dot{\boldsymbol{\Sigma}} + \dot{\gamma} H_{kin} \\ &= \mathbf{n} : \frac{d}{dt}(\|\boldsymbol{\Sigma}\|\mathbf{n}) + \dot{\gamma} H_{kin} = \frac{d}{dt}\|\boldsymbol{\Sigma}\| + \dot{\gamma} H_{kin} \end{aligned}$$

where it has been noted that:

$$\mathbf{n} : \mathbf{n} = 1 \quad \Rightarrow \quad \mathbf{n} : \dot{\mathbf{n}} = \dot{\mathbf{n}} : \mathbf{n} = 0$$

As a result, the limit equation can also be rewritten as:

$$F = h\left[\frac{d}{dt}\|\boldsymbol{\Sigma}\| + \dot{\gamma} H_{kin}\right] - \dot{\gamma}$$

which is a form particularly suitable for an algorithmic implementation of the model.

7.1 Continuous model

Requiring the satisfaction of the continuous limit function $F = 0$, we get:

$$\begin{aligned} F &= h\,[\mathbf{n} : \dot{\mathbf{s}}] - \dot{\gamma} \\ &= h\,[2G(\mathbf{n} : \dot{\mathbf{e}}) - 2G\,\dot{\gamma}] - \dot{\gamma} = 0 \end{aligned}$$

Solving for $\dot{\gamma}$, we obtain:

$$\dot{\gamma} = A^{GP}_{cont}[\mathbf{n} : \dot{\mathbf{e}}]$$

where:

$$A_{cont}^{GP} = \frac{2G}{2G + \dfrac{1}{h(f)}}$$

Note that in the limiting case $f \to \beta$, $h(f) \to (1/H)$, and we regain the classical plasticity model. Moreover, the elasto-plastic stress-strain curve has a continuous slope at the transition point between the elastic and the plastic behavior.

7.2 Discrete algorithmic model

Integrating the continuous limit function over the time interval $[t_n, t_{n+1}]$, we obtain the discrete limit condition:

$$\lambda - h\left[\|\boldsymbol{\Sigma}\| - \|\boldsymbol{\Sigma}_n\| + \lambda\, H_{kin}\right] = 0$$

If we set:

$$\begin{aligned} A_1 &= \|\boldsymbol{\Sigma}^{TR}\| - \sigma_{y,n} \\ A_2 &= \|\boldsymbol{\Sigma}^{TR}\| - \|\boldsymbol{\Sigma}_n\| \\ A_3 &= \delta - 2G \\ A_4 &= (\delta + H)\,\beta \end{aligned}$$

we obtain the quadratic equation:

$$a\lambda^2 + b\lambda + c = 0 \tag{7.1}$$

where:

$$\begin{aligned} a &= 2G_1 A_3 \\ b &= A_4 - A_1 A_3 + 2G_1 A_2 \\ c &= -A_1 A_2 \end{aligned}$$

The physically correct solution corresponds to the smallest positive root. Note that for $\beta = 0$ the model reduces to classical plasticity, as expected. In fact, $\beta = 0$ implies $A_4 = 0$, while $\|\boldsymbol{\Sigma}_n\| \leq \sigma_{y,n}$ implies $A_2 \geq A_1$. Accordingly, equation 7.1 simplifies to:

$$(2G_1\lambda - A_1)\ (A_3\lambda + A_2) = 0$$

which has the roots: $\lambda_1 = -A_2/A_3$, $\lambda_2 = A_1/(2G_1)$. The first root never represents the correct one: in fact for $\delta > 2G$ it is negative; for $0 \leq \delta < 2G$, we have $\lambda_1 > \lambda_2$. On the other hand, the second root is always physically correct and coincides with the root of the classical plasticity model.
If δ and the hardening are both zero, equation 7.1 reduces to:

$$(2G\lambda - A_1)\ (-2G\lambda + A_2) = 0$$

which has the roots: $\lambda_1 = A_2/(2G)$ and $\lambda_2 = A_1/(2G)$. Again λ_2 coincides with the classical plasticity root and $\lambda_1 \geq \lambda_2$; hence, it is the correct solution.

Upon clearing fractions, the discrete limit equation becomes:

$$[\delta(\beta - f) + H\beta]\,\lambda = f\,[\|\boldsymbol{\Sigma}\| - \|\boldsymbol{\Sigma}_n\| + H_{kin}\lambda]$$

Linearizing and noting that:

$$\begin{aligned} d\|\boldsymbol{\Sigma}\| &= \mathbf{n} : d\boldsymbol{\Sigma} = 2G[\mathbf{n} : d\mathbf{e}] - (2G + H_{kin})d\lambda \\ df &= d\|\boldsymbol{\Sigma}\| - H_{iso}d\lambda \end{aligned}$$

we get:

$$d\lambda = A^{GP}_{discr}\,[\mathbf{n} : d\mathbf{e}]$$

where:

$$A^{GP}_{discr} = \frac{2G(B_1 + B_2)}{2G_1B_1 + (2G - \delta)B_2 + B_3}$$

with:

$$\begin{aligned} B_1 &= \|\boldsymbol{\Sigma}\| - \|\boldsymbol{\Sigma}_n\| + (H_{kin} + \delta)\,\lambda \\ B_2 &= \|\boldsymbol{\Sigma}\| - (\sigma_{y,n} + H_{iso}\lambda) = f \\ B_3 &= (\delta + H)\,\beta \end{aligned}$$

Recalling the discussion of Section 4.3, the elasto-plastic tangent tensor consistent with the discrete model can be computed:

$$\mathbf{D}^{GP}_{discr} = \left\{K\ (\mathbf{1}\otimes\mathbf{1}) + 2G\ \left(1 - C^{GP}\right)\ \mathbf{I}_{dev} + \left[2G\ \left(C^{GP} - A^{GP}_{discr}\right)\right](\mathbf{n}\otimes\mathbf{n})\right\}$$

where:

$$C^{GP} = \frac{2G\lambda}{\|\boldsymbol{\Sigma}^{TR}\|}$$

This is a symmetric tensor and for $\beta = 0$ (which implies $B_2 = B_3 = 0$) it returns the classical plasticity tangent tensor.

7.3 Remarks on the model

From a point of view of constitutive behavior, the main features of the generalized plasticity are:

- after initial yield, it shows a smooth transition before reaching an asymptotic value for the stress. The asymptote is horizontal for zero hardening, is not horizontal for non-zero hardening (see figures 7 and 9).
- the speed of the model in reaching the asymptote is controlled by the parameter δ (see figure 8).
- the elasto-plastic stress-strain curve is continuous with its first derivative at the transition point between the elastic and the plastic behavior.
- if unloaded from the plastic range, upon reloading, it renews plasticity before the attainment of the stress where unloading began (see figures 7 and 9).

We wish to stress that this last feature is unique to the GP model and the way in which the model renews plasticity may be easily modified to take into account the behavior of specific real materials. For example, if repeated unloading-loading occurs, without plastic deformation in the reverse direction, for each new loading action an increased value of δ can be progressively used. Depending on the material simulated, the updating formula may be expressed in terms of the distance and the angle between the stresses in correspondence of the successive unloading and reloading (clearly in an appropriate norm). Note that no modification to the discrete algorithm and to the elasto-plastic tangent tensor should be made since the parameter δ is kept constant during all the loading action. Consequently, stress-strain curves of the type represented in figure 10 can be produced; note also that, using update values for δ, the GP model does not collapse toward the perfect plasticity behavior ($f = 0$), when starting from a plastic state with $f > 0$ and a large number of small unloading-reloading are imposed under displacement control.

From an algorithmic point of view, the GP model has a simple implementation; in fact:

- the discrete consistency condition generates a quadratic equation, which can be solved in closed form and for which it is possible to delineate the properties of the roots;
- the elasto-plastic tangent tensor consistent with the discrete model is symmetric.

We wish to conclude stressing that the GP seems to be an extremely versatile model, involving parameters with clear physical meaning. Its algorithmic implementation within a return mapping algorithm is simple and straightforward; in particular, only a few lines of extra code must be added to convert an already implemented CP routine (mainly a specific root for a quadratic equation must be computed). Moreover, the symmetry of the consistent algorithmic elasto-plastic tangent tensor is retained in the discrete setting. Hence, the authors believe that the GP can be successfully used in the simulation of real materials.

8 SPECIALIZATION TO UNI-AXIAL MODELS

All the model discussed so far are three-dimensional, which means that they are defined in terms of general states of stress and strain. Accordingly, the material parameters involved in the constitutive equations (such as the hardening parameters, the yielding stress, etc.) are relative to a three-dimensional setting.

If the reduction of the models to the case of uni-axial states of stress and strain is needed, then the constitutive equations should involve the corresponding one-dimensional quantities, which may be easily computed through the relations:

$$\sigma_y^u = \sqrt{\frac{3}{2}}\sigma_y \ , \quad \beta^u = \sqrt{\frac{3}{2}}\beta \ , \quad \delta^u = \frac{3}{2}\delta$$

$$H_{iso}^u = \frac{2}{3}H_{iso} \ , \quad H_{kin}^u = \frac{2}{3}H_{kin} \ , \quad H_{nl}^u = \frac{2}{3}H_{nl}$$

Just to give an example, note that β measures the distance between the asymptotic and the current radius of the yield function σ_y (for a generic three-dimensional state), while β^u measures the distance between the asymptotic uni-axial stress and σ_y^u.

The material parameters used in the next section for the numerical examples are always expressed in terms of the one-dimensional quantities since they have an easier interpretation.

9 NUMERICAL EXAMPLES

In this section we present some numerical simulations performed to test the models, discussed above; in particular, we concentrate on non-linear kinematic hardening (NLK) and generalized plasticity (GP). All the results are obtained using a three dimensional finite element, based on a *mixed* approach [46] and implemented into the Finite Element Analysis Program (FEAP) [53, 54].

The numerical simulations are organized as follow:

- Cyclic uni-axial test under displacement control: zero mean strain
- Cyclic uni-axial test under displacement control: non-zero mean strain
- Cyclic uni-axial test under force control: zero mean stress
- Cyclic uni-axial test under force control: non-zero mean stress
- Tension-cyclic shear test under displacement control
- Tension-cyclic shear test under force control

For each numerical simulation basically three figures are presented; in the first the stress-strain curve for the NLK model is presented, in the second the same curve for the GP model and in the third one the two previous curves are reported together for the purpose of a direct comparison.

The tests are performed on a cubic specimen of side length equal to 10, with boundary and loading conditions set to produce the appropriate stress/strain state. The sample is modeled with only one element and the material properties are:

$$E = 100 \,, \quad \nu = 0.3 \,, \quad \sigma^u_{y,0} = 15$$

The tests under force control are performed using a special *arc-length* type algorithm to control the time-stepping increments [2].

9.1 Cyclic uni-axial test under displacement control: zero mean strain

The specimen undergoes a cyclic loading history, producing a uni-axial stress (tension-compression). The load is applied controlling the displacements and a zero mean strain is required.

In figure 12 we report the stress-strain curve for the NLK model with parameters:

$$H^u_{kin} = 100 \ , \quad H^u_{nl} = 10 \ , \quad H^u_{iso} = 0$$

For comparison, with dotted lines we present also the solutions of the classical plasticity model for $H^u_{kin} = 0$ and $H^u_{kin} = 100$.

In figure 13 we report the stress-strain curve for the GP model, relatively to the same test, with material parameter:

$$\beta^u = 10 \ , \quad \delta^u = 50 \ , \quad H^u_{kin} = 0 \ , \quad H^u_{iso} = 0$$

while in figure 14 the curves for both models are reported together for comparison purpose.

9.2 Cyclic uni-axial test under displacement control: non-zero mean strain

Again, the specimen is in a uni-axial state of stress (tension-compression) and undergoes a cyclic loading history, controlled through the displacement. But this time, a non-zero mean strain is imposed. The material parameters are the same as in the previous example.

In figures 15, 16 and 17 we report the stress-strain curves for the two models.

9.3 Cyclic uni-axial test under force control: zero mean stress

The specimen undergoes a cyclic loading history, producing a uni-axial state of stress (tension-compression). The load is applied controlling the forces and a zero mean stress is required.

In figure 18 we report the stress-strain curve for the NLK model with parameters:

$$H^u_{kin} = 100 \ , \quad H^u_{nl} = 10 \ , \quad H^u_{iso} = 0$$

In figure 19 we report the stress-strain curve for the GP model, with material parameters:

$$\beta^u = 10 \ , \quad \delta^u = 50 \ , \quad H^u_{kin} = 0 \ , \quad H^u_{iso} = 0$$

while in figure 20 the curves for both models are reported together for comparison purpose.

9.4 Cyclic uni-axial test under force control: non-zero mean stress

For this test the specimen is in a uni-axial state of stress (tension-compression) and undergoes a cyclic loading history, controlled through the applied forces; this time a non-zero mean stress is imposed. The parameter are:

$$H^u_{kin} = 100 \ , \quad H^u_{nl} = 10 \ , \quad H^u_{iso} = 0$$

for the NLK model, and:

$$\beta^u = 20 \ , \quad \delta^u = 5 \ , \quad H^u_{kin} = 5 \ , \quad H^u_{iso} = 0$$

for the GP model.

In figures 21, 22 and 23 we report the stress-strain curves for the two models.

9.5 Tension-cyclic shear test under displacement control

We now want to study the behavior of the two material models for a more complex loading pattern. Therefore, the specimen is subjected first to a uni-axial extension in direction 1 (see figure 24), which produces an axial strain of 0.2. Then a cyclic shear load is applied in direction 2. All the degrees of freedom along the 1 and 2 directions are prescribed during the analysis and the load is applied controlling the displacements.

The parameter are:

$$H^u_{kin} = 100 \ , \quad H^u_{nl} = 10 \ , \quad H^u_{iso} = 0$$

for the NLK model, and:

$$\beta^u = 10\,, \quad \delta^u = 50\,, \quad H^u_{kin} = 0\,, \quad H^u_{iso} = 0$$

for the GP model. The shear stress-strain curves are presented in figures 25, 26 and 27.

9.6 Tension-cyclic shear test under force control

The test is conceptually identical to the previous one, except that the specimen is under force control. The only restrained degrees of freedom are those to prevent rigid body motions. The applied tension load produces an axial stress of 4. The parameter are:

$$H^u_{kin} = 100\,, \quad H^u_{nl} = 10\,, \quad H^u_{iso} = 0$$

for the NLK model, and:

$$\beta^u = 10\,, \quad \delta^u = 50\,, \quad H^u_{kin} = 0\,, \quad H^u_{iso} = 0$$

for the GP model. The shear stress-strain curves are presented in figures 28, 29 and 30.

10 SUMMARY

In this Section we summarize the basic equations and results of the paper.

Continuous model

$$\dot{\boldsymbol{\sigma}} = \mathbf{D}_{cont}\dot{\boldsymbol{\epsilon}}$$

$$\mathbf{D}_{cont} = \{K\,(\mathbf{1}\otimes\mathbf{1}) + 2G\,[\mathbf{I}_{dev} - A_{cont}(\mathbf{n}\otimes\mathbf{n})]\}$$

$$\dot{\gamma} = A_{cont}[\mathbf{n} : \dot{\mathbf{e}}]$$

Discrete model

$$d\boldsymbol{\sigma} = \mathbf{D}_{discr}\,d\boldsymbol{\epsilon}$$

$$\mathbf{D}_{discr.} = K\,(\mathbf{1}\otimes\mathbf{1}) + 2G\,(1-C)\,\mathbf{I}_{dev}$$
$$+ [2G\,(C - A_{discr}) + B(\mathbf{n} : \boldsymbol{\alpha})]\,(\mathbf{n}\otimes\mathbf{n}) - B(\boldsymbol{\alpha}\otimes\mathbf{n})$$

$$
\begin{aligned}
B &= A_{discr} T^{\lambda} C H_{nl} \\
C &= \frac{2G\lambda}{\|\boldsymbol{\Sigma}_A^{\lambda}\|} \\
d\lambda &= A_{discr}\,[\mathbf{n} : d\mathbf{e}]
\end{aligned}
$$

Material model	Continuous version	Discrete version
CP	$A_{cont}^{CP} = \dfrac{2G}{2G_1}$	$A_{discr}^{CP} = \dfrac{2G}{2G_1}$ $\lambda^{CP} = \dfrac{\|\boldsymbol{\Sigma}^{TR}\| - \sigma_{y,n}}{2G_1}$ $B = 0$
NLK	$A_{cont}^{NLK} = \dfrac{2G}{2G_1 - H_{nl}[\mathbf{n} : \boldsymbol{\alpha}]}$	$A_{discr}^{NLK} = \dfrac{2G}{2G_0 + T^{\lambda} H_{kin} - T^{\lambda} H_{nl}(\mathbf{n} : \boldsymbol{\alpha})}$
GP	$A_{cont}^{GP} = \dfrac{2G}{2G + \dfrac{1}{h(f)}}$	$A_{discr}^{GP} = \dfrac{2G(B_1 + B_2)}{2G_1 B_1 + (2G - \delta)B_2 + B_3}$

Recall that:

$$
\begin{aligned}
2G_0 &= 2G + H_{iso} \\
2G_1 &= 2G + H_{iso} + H_{kin}
\end{aligned}
$$

11 CLOSURE

In this paper we present a comparative study between the non-linear kinematic hardening (NLK) model and the generalized plasticity (GP) model, which are both capable of simulation of real material behavior under cyclic loading conditions.

We discuss the models from a continuous and a discrete time point of view, presenting their algorithmic implementation within a return mapping framework. The form of the elasto-plastic tangent tensor consistent with the continuous and the discrete versions of the model is also presented.

The NLK has already been used in the simulation of the behavior of some metals under cyclic loading paths, achieving an high degree of accuracy. Extensions of the model have been presented to include strain range memory,

visco-plastic recovery properties, ratcheting effects [4, 5, 7, 8, 6, 9, 26]. However, difficulties arise to consistently implement the model in a return mapping framework. The discrete consistency condition yields a quartic equation, with coefficients a function of the trial state and the previous solution, which makes the search for the minimum positive root difficult. A robust approach based on a combination of a Newton algorithm and a synthetic division is presented, which makes the model computationally expensive, compared to generalized plasticity. Moreover, the elasto-plastic tangent tensor consistent with the discrete model is non-symmetric and, consequently, an appropriate solver must be used, plus the required array storage is doubled.

On the other hand, if compared to the NLK, the generalized plasticity is a fairly new model. It possesses interesting features, such as: the presence of two different parameter (β and δ) with clear physical meaning, measuring respectively the limiting values of reachable stress and the speed in reaching this ultimate value. Moreover, if unloaded from a plastic state and reloaded before the occurrence of plastic deformation in the reverse direction, the GP can renew plasticity at a value of the stress lower than the one at which the unload began. This last feature is unique to the GP and can be properly modified to closely simulate specific materials. Algorithmically, the model has a simple and straightforward implementation since the discrete consistency condition generates a quadratic equation and the elasto-plastic tangent tensor consistent with the discrete model is symmetric. These features make the authors believing that the GP can be successfully used in the simulation of real materials.

Acknowledgement

The authors would like to acknowledge Professor J.Lubliner for many useful discussions on the generalized plasticity model and Professor P.Papadopoulos for a discussion of the loading/unloading conditions of infinitesimal discrete elasto-plasticity [39].

References

[1] P.J. Armstrong and C.O. Frederick, *A mathematical representation of the multi-axial baushinger effect*, Tech. Report C.E.G.B. Report RD/B/N731, Berkeley Nuclear Laboratories, R&D Department, 1966.

[2] F. Auricchio and R.L. Taylor, *A simple automatic time-stepping algorithm for cyclic non-linear problems*, Report UCB/SEMM-93, Department of Civil Engineering, University of California at Berkeley, 1993, to be published.

[3] F. Auricchio, R.L. Taylor, and J. Lubliner, *Application of a return map algorithm to plasticity models*, COMPLAS Computational Plasticity: Fundamentals and Applications (Barcelona) (D.R.J. Owen and E. Onate, eds.), 1992, pp. 2229–2248.

[4] J.L. Chaboche, *Time independent constitutive theories for cyclic plasticity*, International Journal of Plasticity **2** (1986), 149–188.

[5] ———, *Constitutive equations for cyclic plasticity and cyclic viscoplasticity*, International Journal of Plasticity **5** (1989), 247–302.

[6] ———, *On some modifications of kinematic hardening to improve the description of ratcheting effects*, International Journal of Plasticity **7** (1991), 661–678.

[7] J.L. Chaboche and D. Nouailhas, *Constitutive modeling of ratcheting effects - Part I: experimental facts and properties of the classical models*, Journal of Engineering Materials and Technology **111** (1989), 384–392.

[8] ———, *Constitutive modeling of ratcheting effects - Part II: possibilities of some additional kinematic rules*, Journal of Engineering Materials and Technology **111** (1989), 409–416.

[9] J.L. Chaboche, D. Nouailhas, D. Pacou, and P. Paulmier, *Modeling of the cyclic response and ratcheting effects on Inconel-718 alloy*, European Journal of Mechanics - A:Solids **10** (1991), 101–121.

[10] Y.F. Dafalias, *Bounding surface plasticity. I: mathematical foundation and hypoplasticity*, Journal of Engineering Mechanics **112** (1986), 966–987.

[11] ———, *Bounding surface plasticity model for steel under cyclic loading*, Cyclic buckling of steel structures and structural elements under dynamic loading conditions (Osaka, Japan), U.S.-Japan Seminar, 1991, pp. 1–12.

[12] Y.F. Dafalias and E.P. Popov, *A model of nonlinearly hardening materials for complex loading*, Acta Mechanica **21** (1975), 173–192.

[13] ———, *Plastic internal variables formalism of cyclic plasticity*, Journal of Applied Mechanics **43** (1976), 645–651.

[14] I. Doghri, *Fully implicit integration and consistent tangent modulus in elasto-plasticity*, Private Communication, 1992.

[15] D.C. Drucker and L. Palgen, *On stress-strain relations suitable for cyclic and other loading*, Journal of Applied Mechanics **48** (1981), 479–485.

[16] M.A. Eisenberg, *A generalization of plastic flow theory with application to cyclic hardening softening phenomena*, Journal of Engineering Materials and Technology **98** (1976), 221–228.

[17] M.A. Eisenberg and A. Phillips, *On nonlinear kinematic hardening*, Acta Mechanica **5** (1968), 1–13.

[18] ———, *A theory of plasticity with non-coincident yield and loading surfaces*, Acta Mechanica **11** (1971), 247–260.

[19] S.P. Engelstad, S.K. Jain, and J.N. Reddy, *On the application of incremental theory of plasticity with endochronic hardening rule*, COMPLAS Computational Plasticity: Fundamentals and Applications (Barcelona) (D.R.J.Owen and E.Onate, eds.), 1992, pp. 271–282.

[20] T. Hassam, E. Corona, and S. Kyriakides, *Ratcheting in cyclic plasticity, part II: multi-axial behavior*, International Journal of Plasticity **8** (1992), 117–146.

[21] T. Hassam and S. Kyriakides, *Ratcheting in cyclic plasticity, part I: uniaxial behavior*, International Journal of Plasticity **8** (1992), 91–116.

[22] M. Klisinki, Z. Mroz, and K. Runesson, *Structure of constitutive equations in plasticity for different choices of state and control variables*, International Journal of Plasticity **8** (1992), 221–243.

[23] R.D. Krieg and D.B. Krieg, *Accuracies of numerical solution methods for the elastic-perfectly plastic model*, Journal of Pressure Vessel Technology, Transaction of ASME (1977), 510–515.

[24] H.S. Lamba and O.M. Sidebottom, *Cyclic plasticity for non-proportional paths. Part 1: cyclic hardening, erasure of memory, and subsequent strain hardening experiments*, Journal of Engineering Materials and Technology **100** (1978), 96–103.

[25] ———, *Cyclic plasticity for non-proportional paths. Part 2: comparison with predictions of three incremental plasticity models*, Journal of Engineering Materials and Technology **100** (1978), 104–111.

[26] J. Lemaitre and J.L. Chaboche, *Mechanics of solid materials*, Cambridge University Press, 1990.

[27] J.D. Lubahn, *Baushinger effect in creep and tensile tests on copper*, Journal of Metals (1955), 1031–1033.

[28] J. Lubliner, *Plasticity theory*, Macmillan, 1990.

[29] ———, *A simple model of generalized plasticity*, International Journal of Solids and Structures **28** (1991), 769–778.

[30] J. Lubliner, R.L. Taylor, and F. Auricchio, *A new model of generalized plasticity*, submitted for publication.

[31] G. Maenchen and S. Sack, *The tensor code*, Methods in computational physics (B. Alder, ed.), vol. 3, Academic Press, 1964, pp. 181–210.

[32] D.L. McDowell, *An evaluation of recent developments in hardening and flow rules for rate-independent non-proportional cyclic plasticity*, Journal of Applied Mechanics **54** (1987), 323–334.

[33] ———, *A non-linear kinematic hardening theory for cyclic thermoplasticity and thermo-visco-plasticity*, International Journal of Plasticity **8** (1992), 695–728.

[34] Z. Mroz, *On the description of anisotropic work-hardening*, Journal of the Mechanics and Physics of Solids **15** (1967), 163–175.

[35] ———, *An attempt to describe the behavior of metals under cyclic loads using a more general work hardening model*, Acta Mechanica **7** (1969), 199–212.

[36] Z. Mroz, H.P. Shrivastava, and R.N. Dubey, *A non-linear hardening model and its application to cyclic loading*, Acta Mechanica **25** (1976), 51–61.

[37] P.M. Naghdi and D.J. Nikkel, *Calculations for uniaxial stress and strain cycling in plasticity*, Journal of Applied Mechanics **51** (1984), 481–493.

[38] J.C. Nagtegaal, *On the implementation of inelastic constitutive equations with special reference to large deformation problems*, Computer Methods in Applied Mechanics and Engineering **33** (1982), 469–484.

[39] P. Papadopoulos and R.L. Taylor, *On the loading/unloading conditions of infinitesimal discrete elasto-plasticity*, submitted for publication.

[40] A. Phillips and R.L. Sierakowski, *On the concept of yield surface*, Acta Mechanica **1** (1965), 29–35.

[41] W.H. Press, B.P. Flannery, S.A. Teukolsky, and W.T. Vetterliy, *Numerical recipes in C: the art of computing*, Cambridge University Press, 1988.

[42] R.L. Sierakowski and A. Phillips, *The effect of repeated loading on the yield surface*, Acta Mechanica **6** (1968), 217–231.

[43] J.C. Simo and S. Govindjee, *Non-linear B-stability and symmetry preserving return mapping algorithms for plasticity and visco-plasticity*, International Journal for Numerical Methods in Engineering **31** (1991), 151–176.

[44] J.C. Simo and T.J.R. Hughes, *Elasto-plasticity and visco-plasticity: computational aspects*, Springer-Verlag, 1993, to be published.

[45] J.C. Simo and R.L. Taylor, *Consistent tangent operators for rate-independent elasto-plasticity*, Computer Methods in Applied Mechanics and Engineering **48** (1985), 101–118.

[46] J.C. Simo, R.L. Taylor, and K.S. Pister, *Variational and projection methods for the volume constraint in finite deformation elasto-plasticity*, Computer Methods in Applied Mechanics and Engineering **51** (1985), 177–208.

[47] K.C. Valanis, *A theory of visco-plasticity without a yield surface. Part I. general theory*, Archives of Mechanics **23** (1971), 517–533.

[48] _____, *A theory of visco-plasticity without a yield surface. Part II. application to mechanical behavior of metals*, Archives of Mechanics **23** (1971), 535–551.

[49] _____, *Fundamental consequences of a new intrinsic time measure. plasticity as a limit case of the endochronic theory*, Archives of Mechanics **32** (1980), 171–191.

[50] O. Watanabe and S.N. Atluri, *Constitutive modeling of cyclic plasticity and creep, using an internal time concept*, International Journal of Plasticity **2** (1986), 107–134.

[51] _____, *Internal time, general internal variables and multi-yield-surface theories of plasticity and creep: a unification of concepts*, International Journal of Plasticity **2** (1986), 37–57.

[52] M.L. Wilkins, *Calculation of elastic plastic flow*, Methods in computational physics (B. Alder, ed.), vol. 3, Academic Press, 1964, pp. 211–263.

[53] O.C. Zienkiewicz and R.L. Taylor, *The finite element method*, fourth ed., vol. I, McGraw Hill, New York, 1989.

[54] _____, *The finite element method*, fourth ed., vol. II, McGraw Hill, New York, 1991.

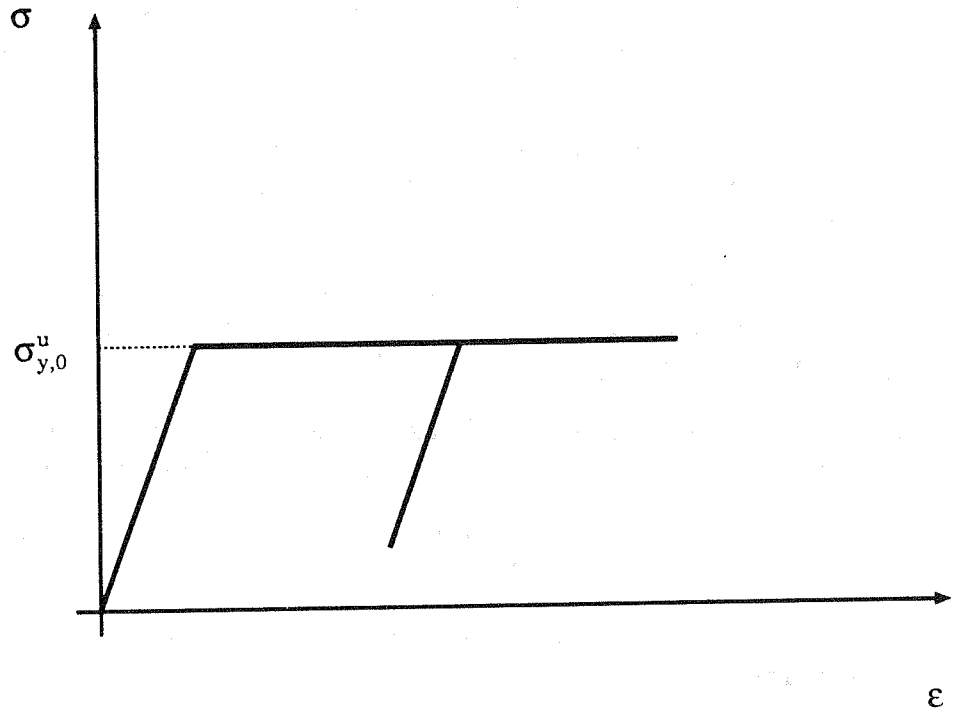

Figure 1: Classical plasticity (CP) with no hardening. Uni-axial stress σ versus uni-axial strain ϵ. If unloaded from the plastic range and reloaded before occurrence of plasticity in the reverse direction, the model renews plasticity at the same stress where unloading began.

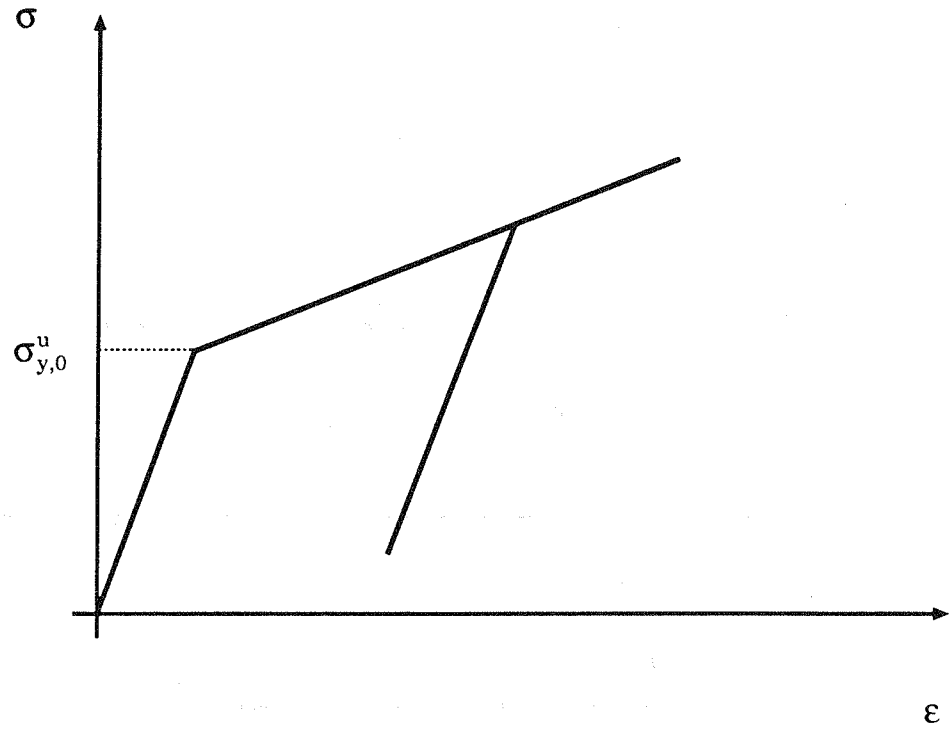

Figure 2: Classical plasticity (CP) with hardening. Uni-axial stress σ versus uni-axial strain ϵ. If unloaded from the plastic range and reloaded before occurrence of plasticity in the reverse direction, the model renews plasticity at the same stress where unloading began.

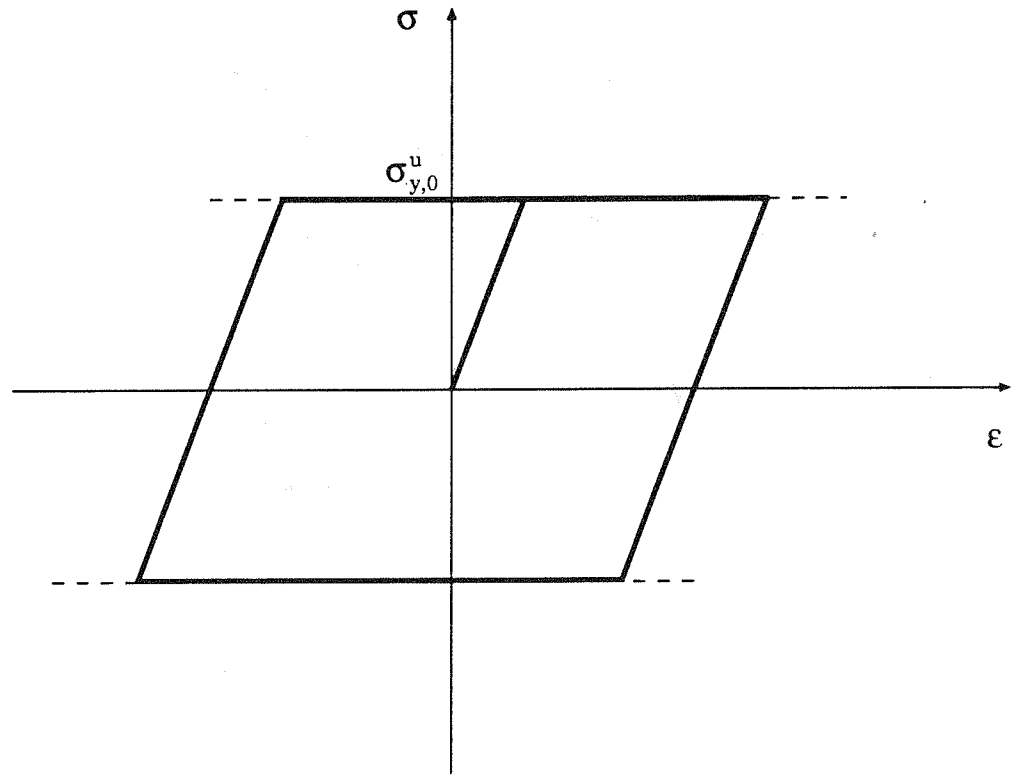

Figure 3: Classical plasticity (CP) with no hardening under cyclic loading condition. Uni-axial stress σ versus uni-axial strain ϵ.

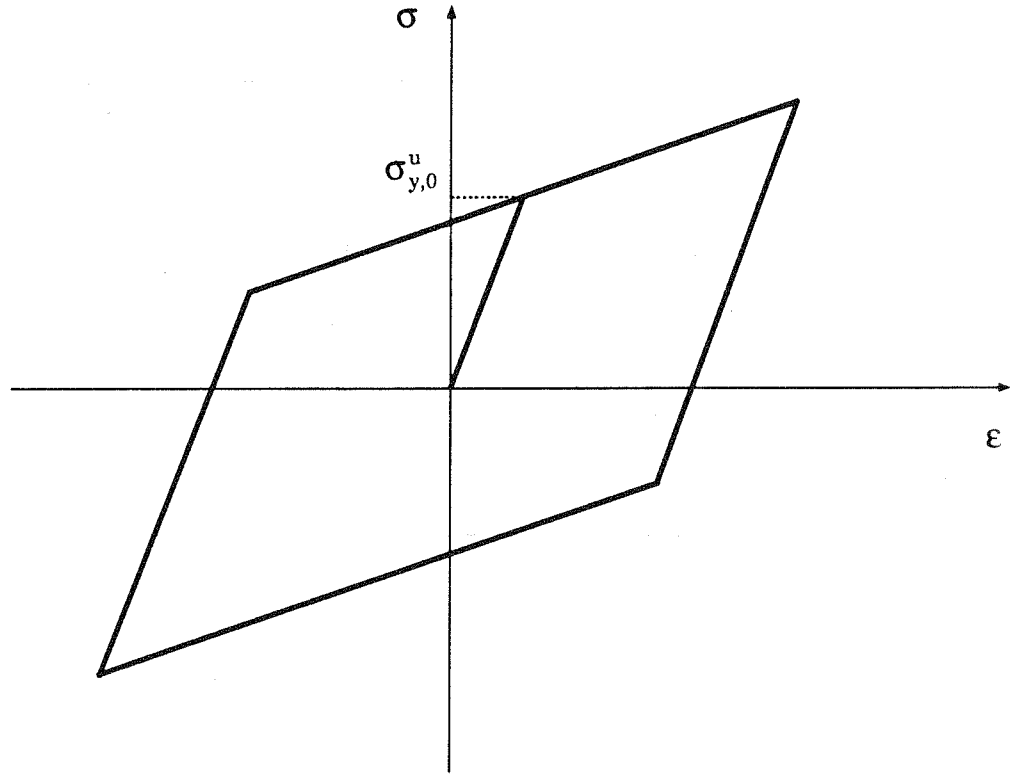

Figure 4: Classical plasticity (CP) with hardening under cyclic loading condition. Uni-axial stress σ versus uni-axial strain ϵ.

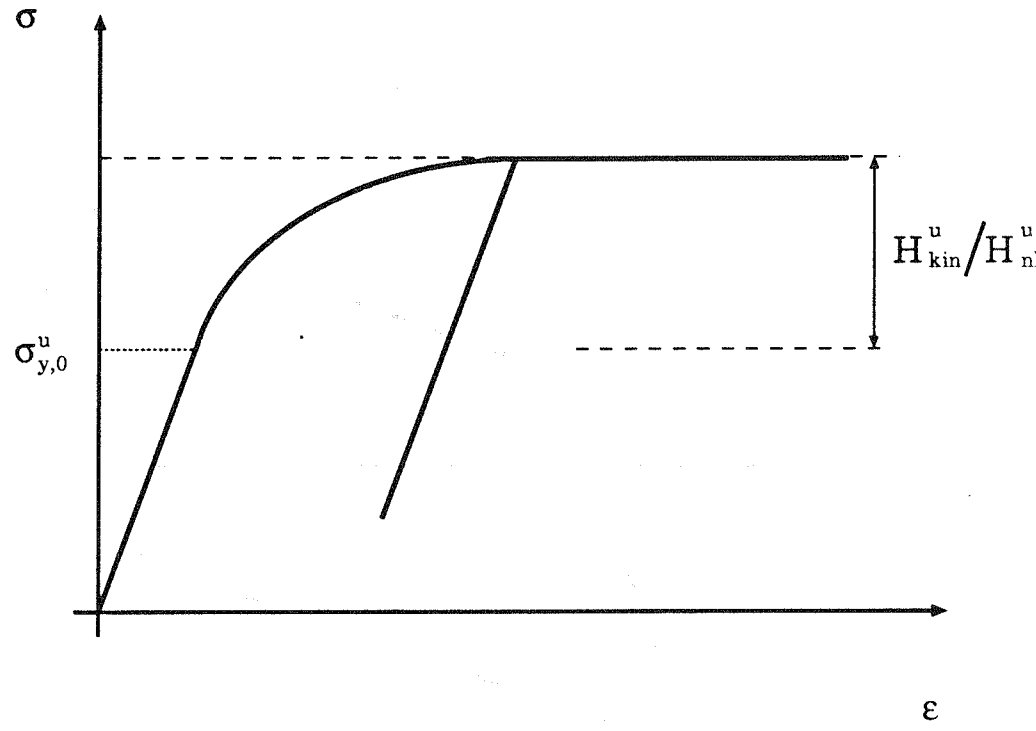

Figure 5: Non-linear kinematic hardening model (NLK). Uni-axial stress σ versus uni-axial strain ϵ. the model shows a smooth transition to a horizontal asymptote and, if unloaded from the plastic range and reloaded before the occurrence of reverse plasticity, it renews plasticity exactly at the same stress where unloading began.

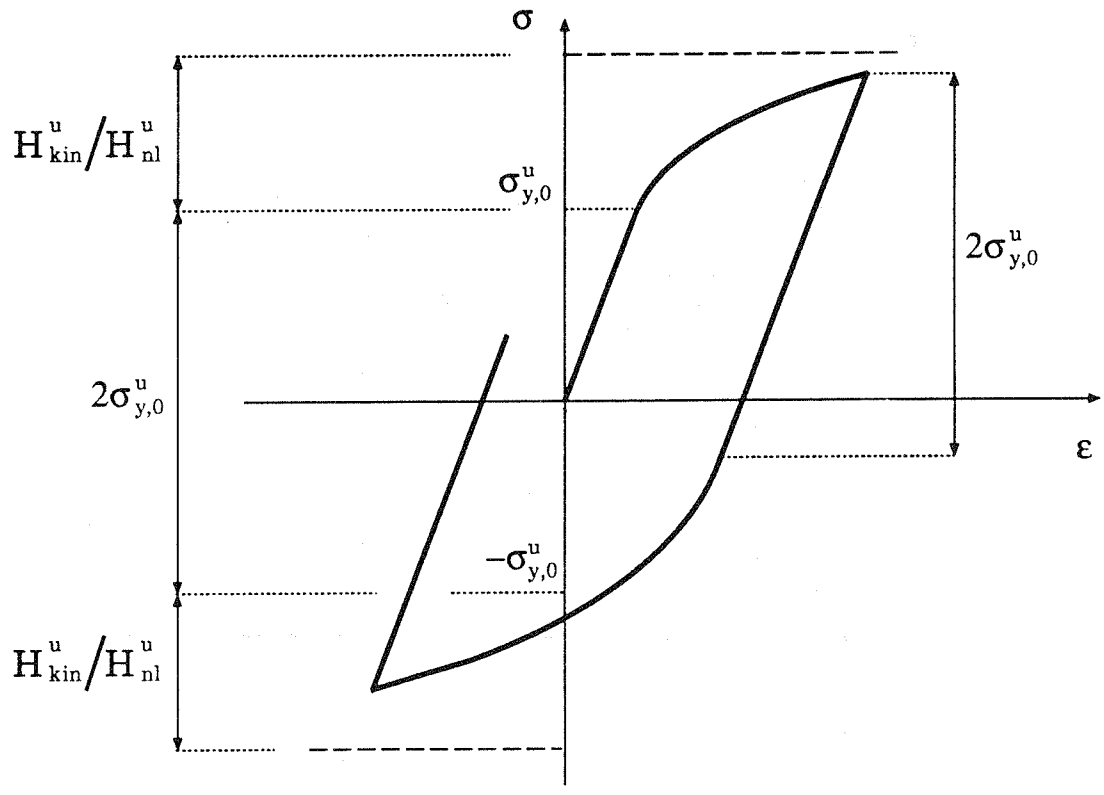

Figure 6: Non-linear kinematic hardening model (NLK) under cyclic loading condition. Uni-axial stress σ versus uni-axial strain ϵ. The model retains its capacity of smooth transition between elastic and plastic behavior also under cyclic load.

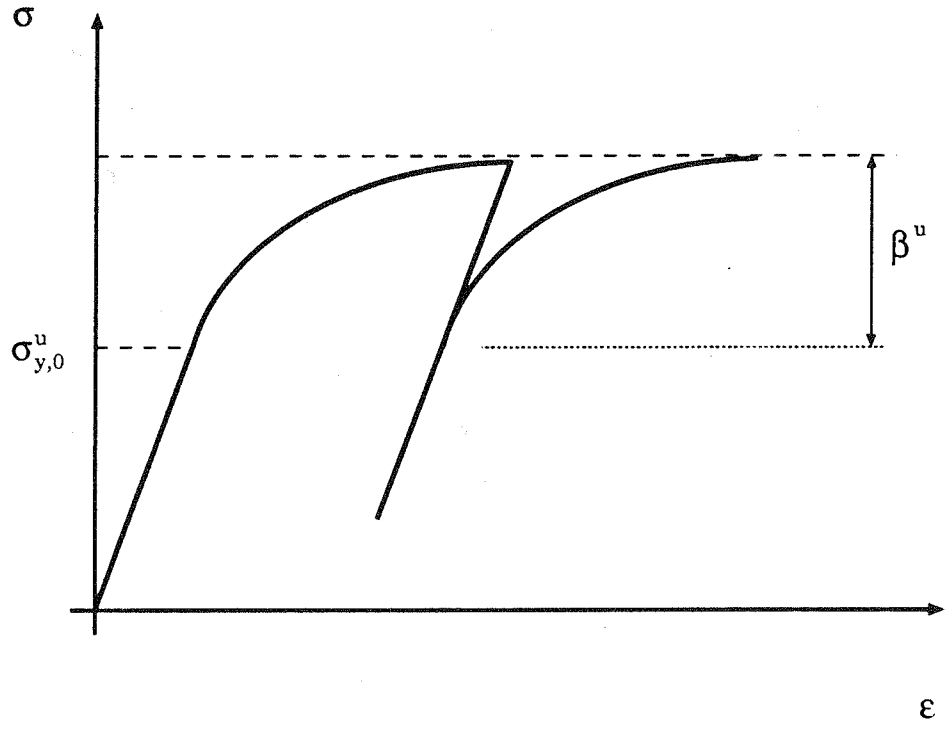

Figure 7: Generalized plasticity model (GP) with no hardening. Uni-axial stress σ versus uni-axial strain ϵ. If unloaded from the plastic range and reloaded before the occurrence of reverse plasticity, the model renews plasticity before the attainment of the stress at which the unloading began.

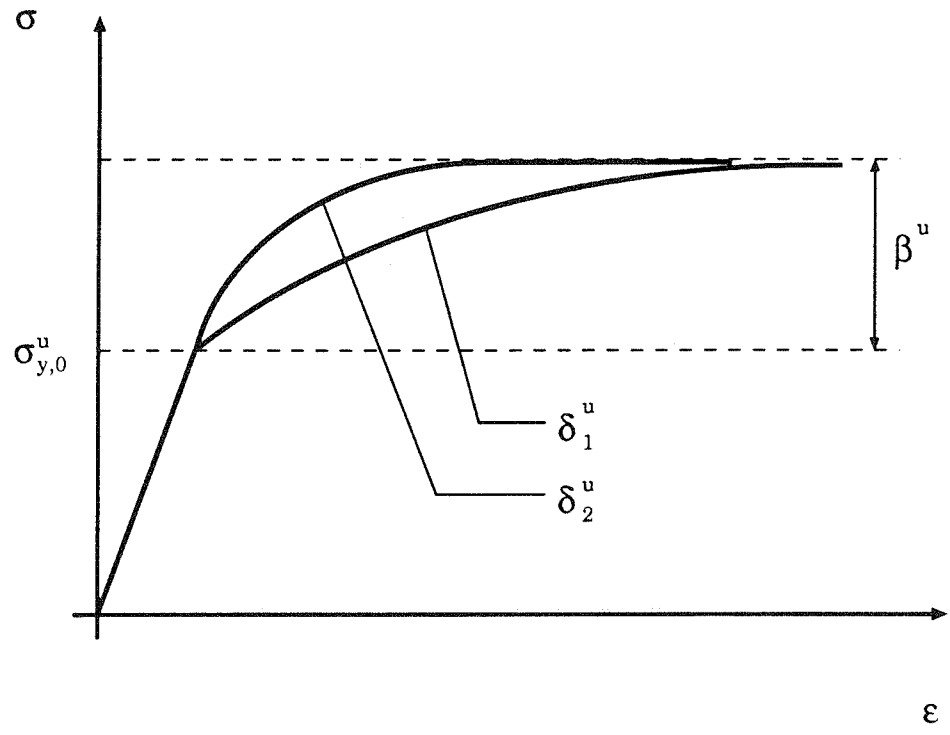

Figure 8: Generalized plasticity model (GP) with no hardening. Uni-axial stress σ versus uni-axial strain ϵ for different values of the parameter δ^u ($\delta^u{}_1 < \delta^u{}_2$).

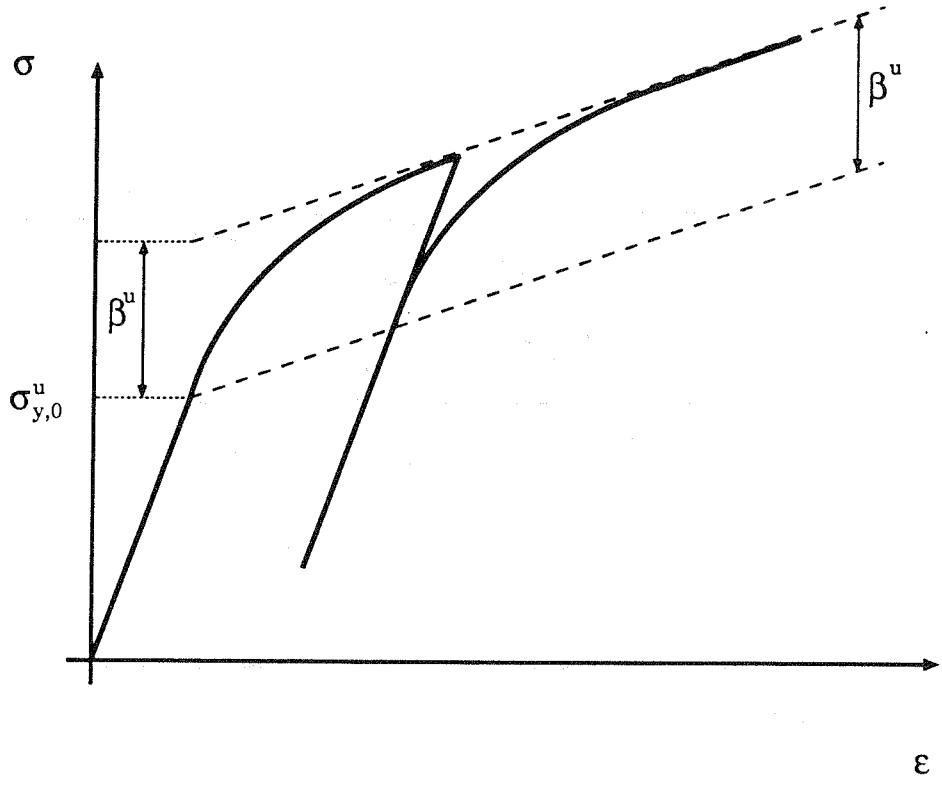

Figure 9: Generalized plasticity model (GP) with non-zero hardening. Uni-axial stress σ versus uni-axial strain ϵ. The model reaches a non-horizontal asymptote and, if unloaded from the plastic range and reloaded before the occurrence of reverse plasticity, it renews plasticity before the attainment of the stress at which the unloading began.

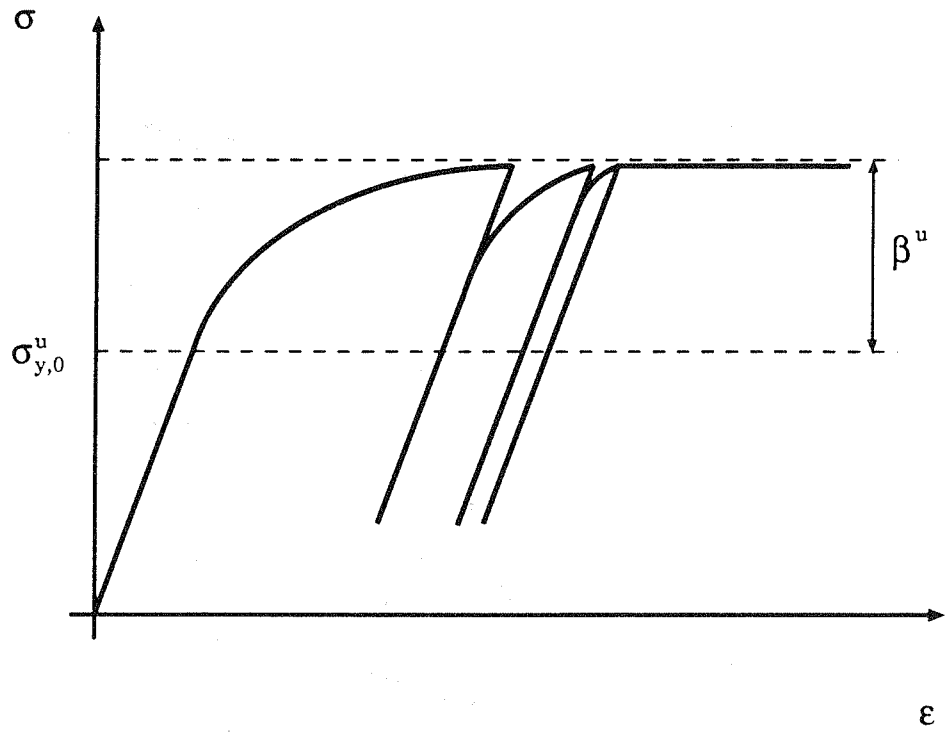

Figure 10: Generalized plasticity model (GP) with no hardening and update for the δ parameter. Uni-axial stress σ versus uni-axial strain ϵ.

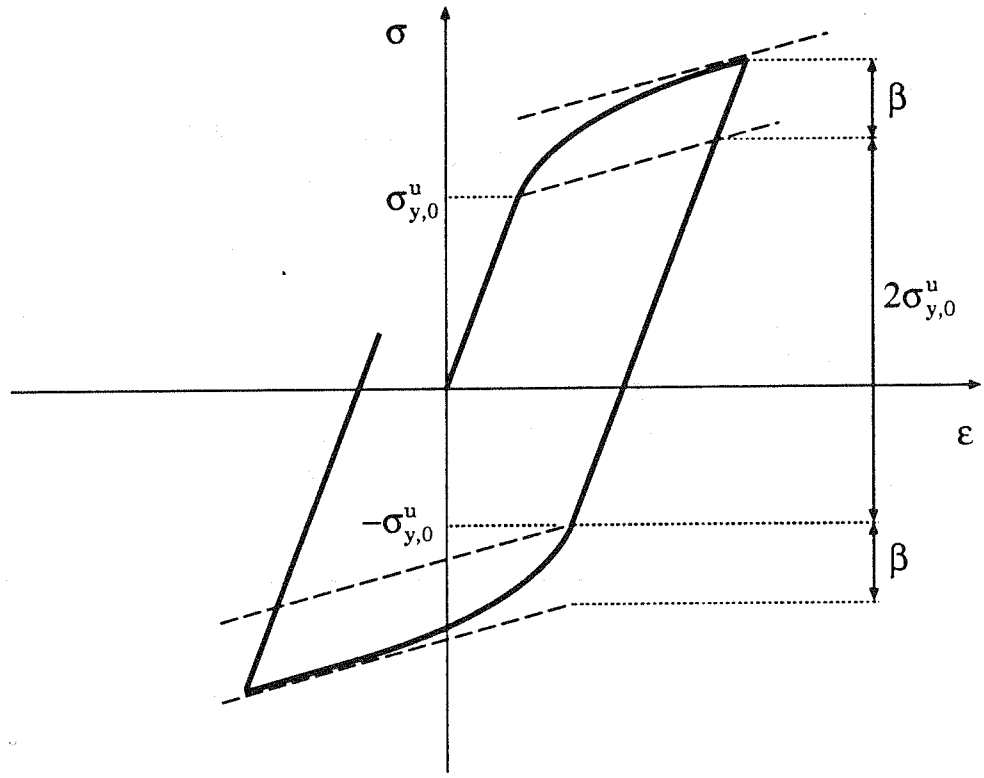

Figure 11: Generalized plasticity model (GP) under cyclic loading condition. Uni-axial stress σ versus uni-axial strain ϵ.

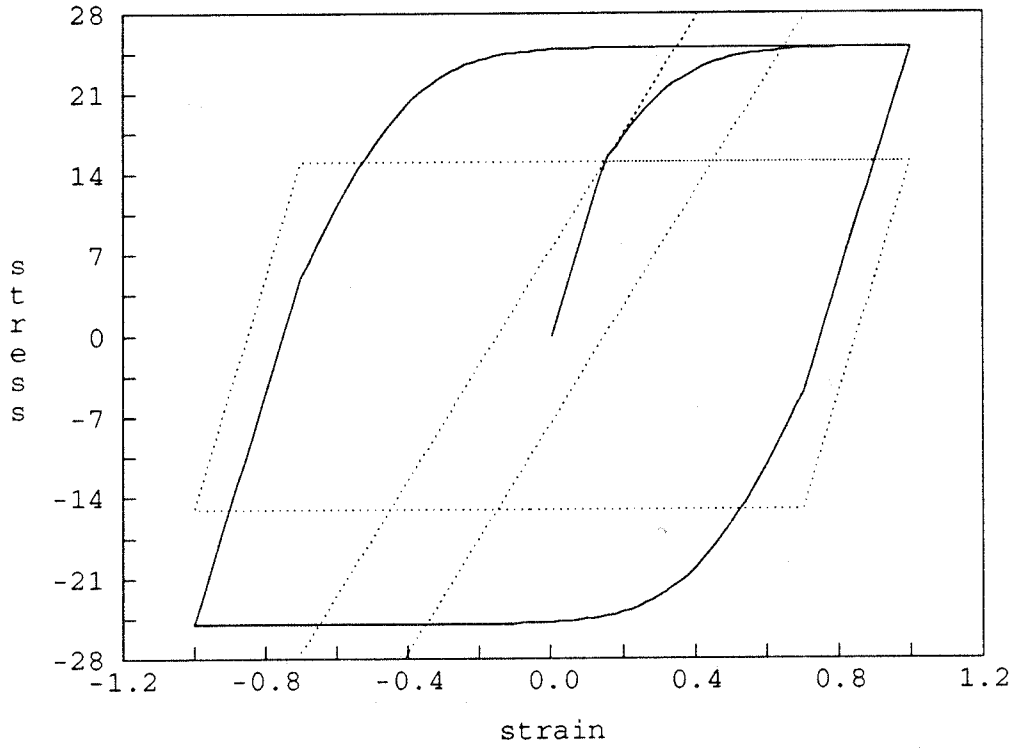

Figure 12: Non-linear kinematic hardening model (NLK) under cyclic uni-axial load (displacement control, zero mean strain). Uni-axial stress σ versus uni-axial strain ϵ.
$\sigma^u_{y,0} = 15$, $H^u_{kin} = 100$, $H^u_{nl} = 10$, $H^u_{iso} = 0$
For comparison, with dotted lines we present also the solutions of the classical plasticity model for $H^u_{kin} = 0$ and $H^u_{kin} = 100$.

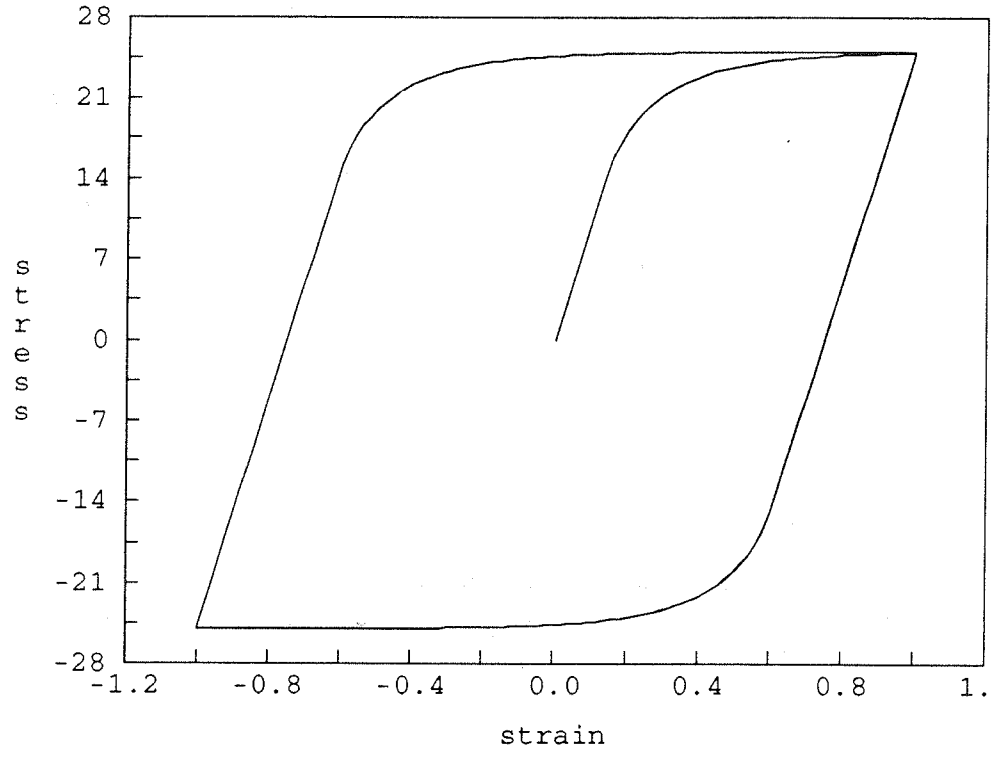

Figure 13: Generalized plasticity (GP) under cyclic uni-axial load (displacement control, zero mean strain). Uni-axial stress σ versus uni-axial strain ϵ. $\sigma^u_{y,0} = 15$, $\beta^u = 10$, $\delta^u = 50$, $H^u_{kin} = 0$, $H^u_{iso} = 0$.

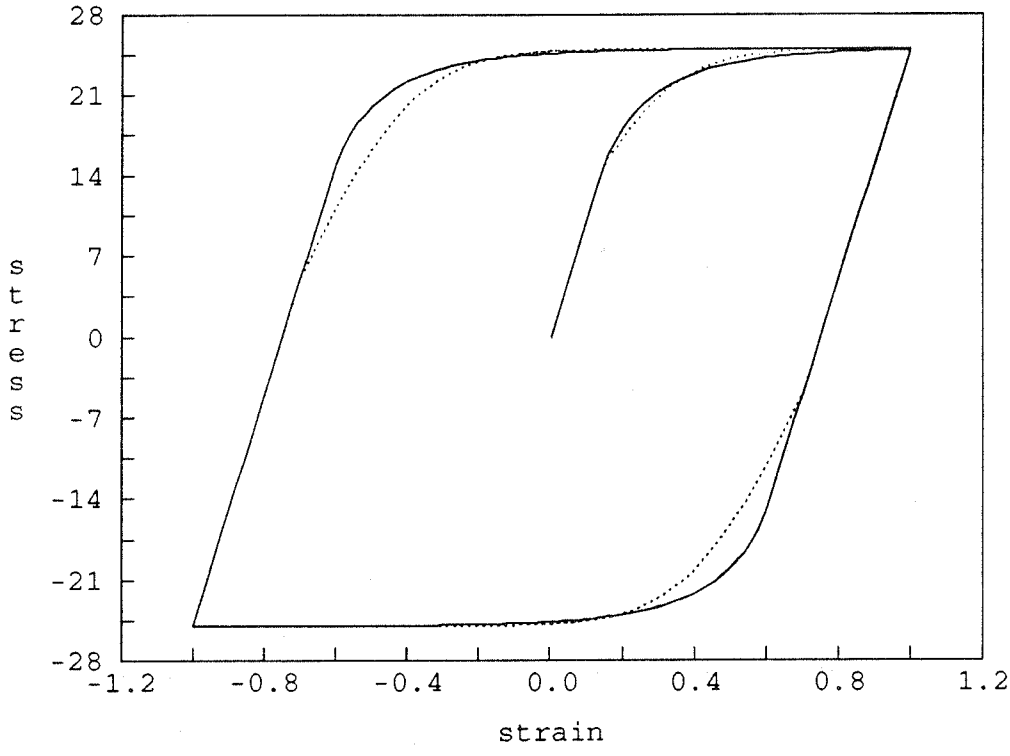

Figure 14: Generalized plasticity (GP) [continuous line] versus non-linear kinematic hardening (NLK) [dotted line] under cyclic uni-axial load (displacement control, zero mean strain). Uni-axial stress σ versus uni-axial strain ϵ.

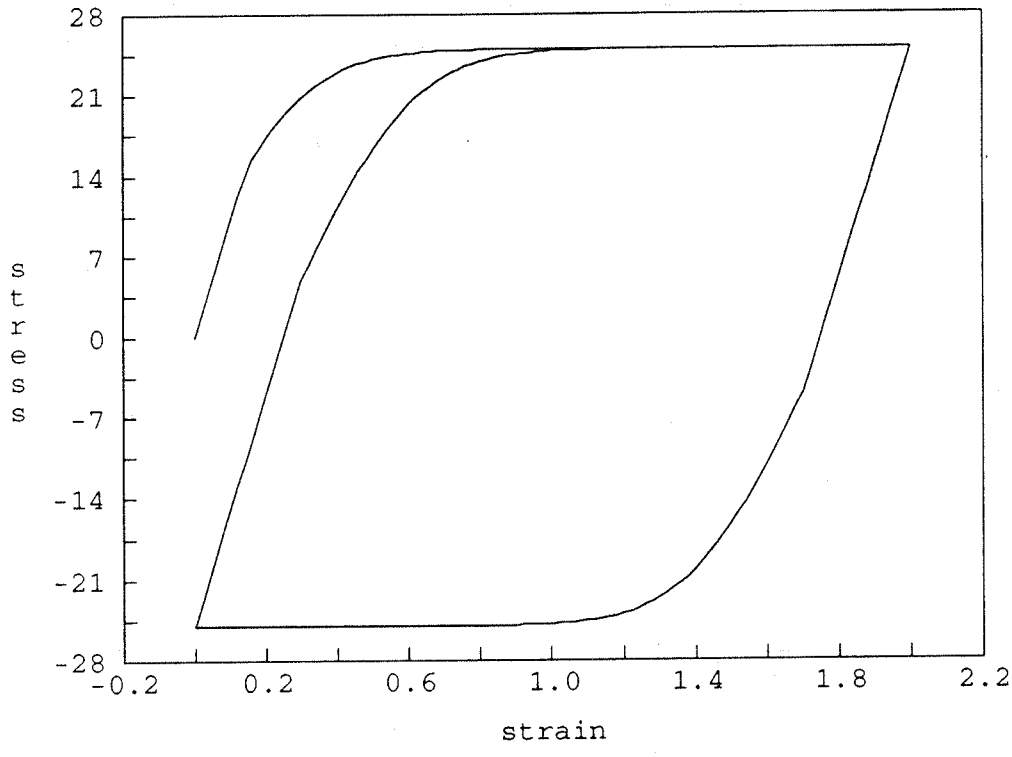

Figure 15: Non-linear kinematic hardening model (NLK) under cyclic uni-axial load (displacement control, non-zero mean strain). Uni-axial stress σ versus uni-axial strain ϵ.
$\sigma^u_{y,0} = 15$, $H^u_{kin} = 100$, $H^u_{nl} = 10$, $H^u_{iso} = 0$

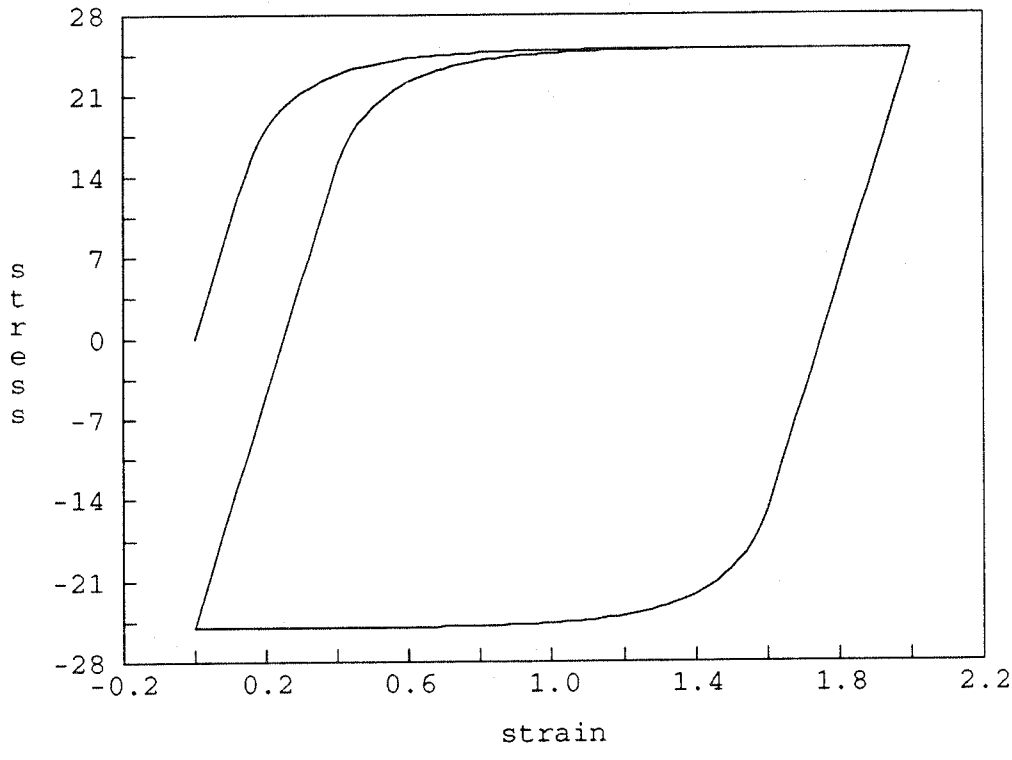

Figure 16: Generalized plasticity (GP) under cyclic uni-axial load (displacement control, non-zero mean strain). Uni-axial stress σ versus uni-axial strain ϵ.
$\sigma^u_{y,0} = 15$, $\beta^u = 10$, $\delta^u = 50$, $H^u_{kin} = 0$, $H^u_{iso} = 0$.

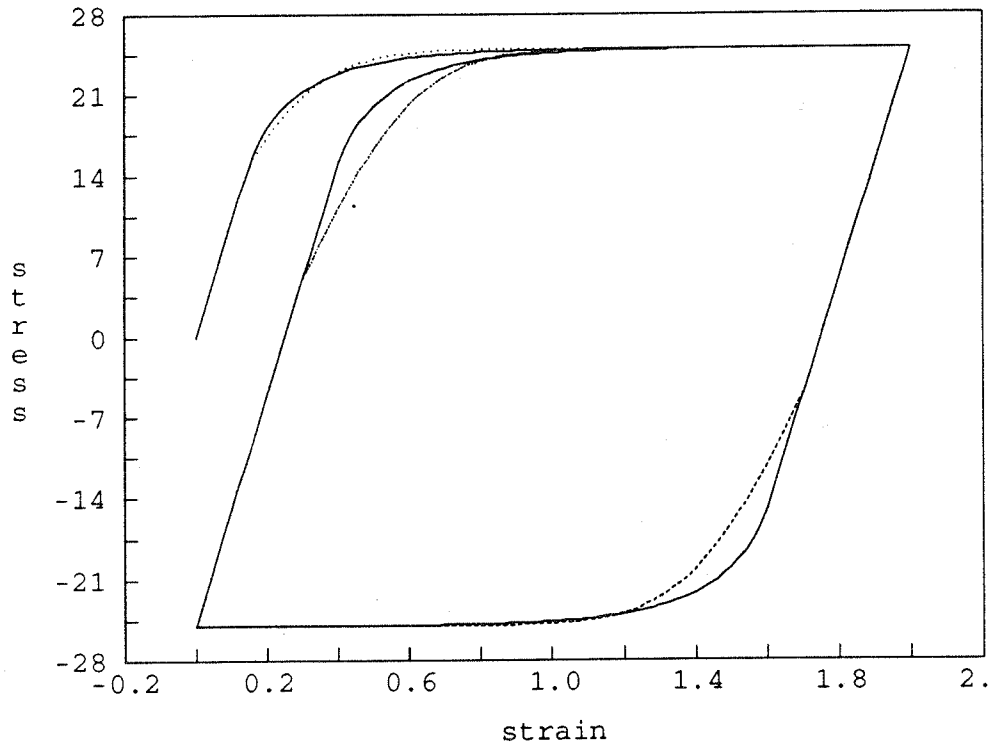

Figure 17: Generalized plasticity (GP) [continuous line] versus non-linear kinematic hardening (NLK) [dotted line] under cyclic uni-axial load (displacement control, non-zero mean strain). Uni-axial stress σ versus uni-axial strain ϵ.

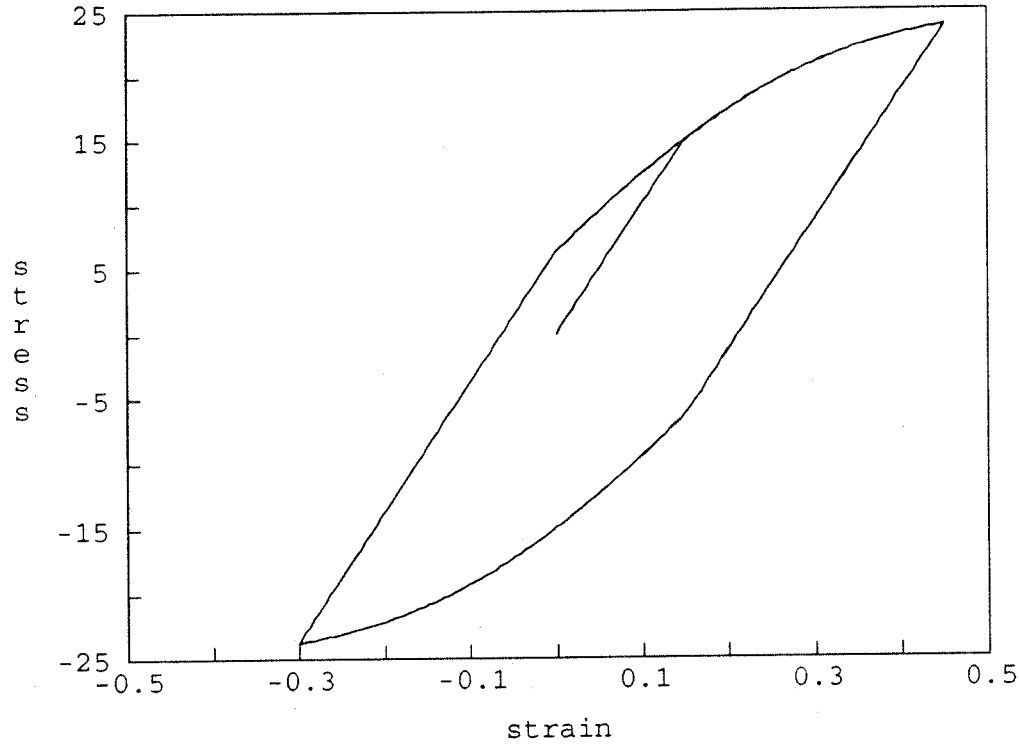

Figure 18: Non-linear kinematic hardening model (NLK) under cyclic uni-axial load (force control, zero mean stress). Uni-axial stress σ versus uni-axial strain ϵ.
$\sigma^u_{y,0} = 15$, $H^u_{kin} = 100$, $H^u_{nl} = 10$, $H^u_{iso} = 0$

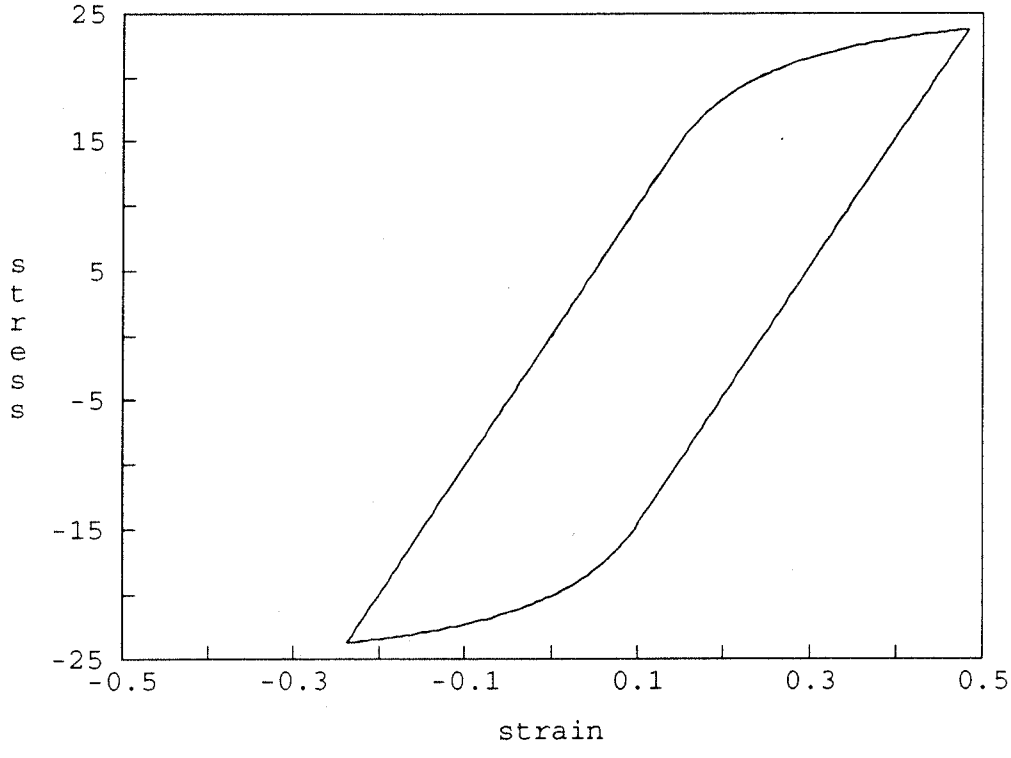

Figure 19: Generalized plasticity (GP) under cyclic uni-axial load (force control, zero mean stress). Uni-axial stress σ versus uni-axial strain ϵ. $\sigma^u_{y,0} = 15$, $\beta^u = 10$, $\delta^u = 50$, $H^u_{kin} = 0$, $H^u_{iso} = 0$.

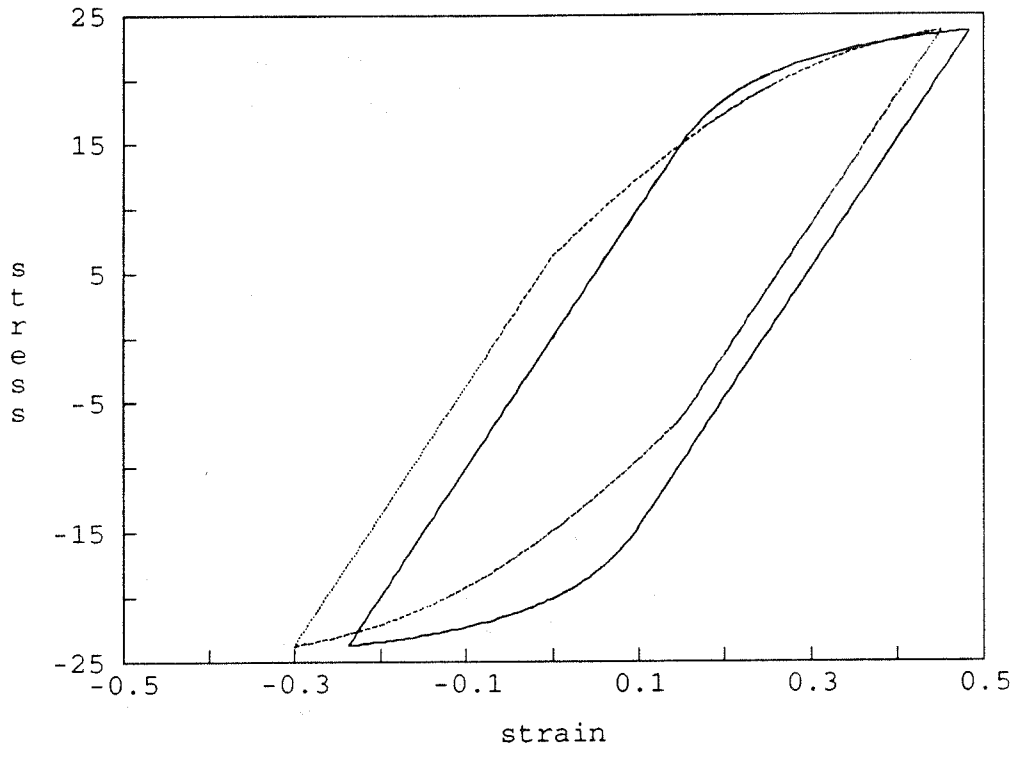

Figure 20: Generalized plasticity (GP) [continuous line] versus non-linear kinematic hardening (NLK) [dotted line] under cyclic uni-axial load (force control, zero mean stress). Uni-axial stress σ versus uni-axial strain ϵ.

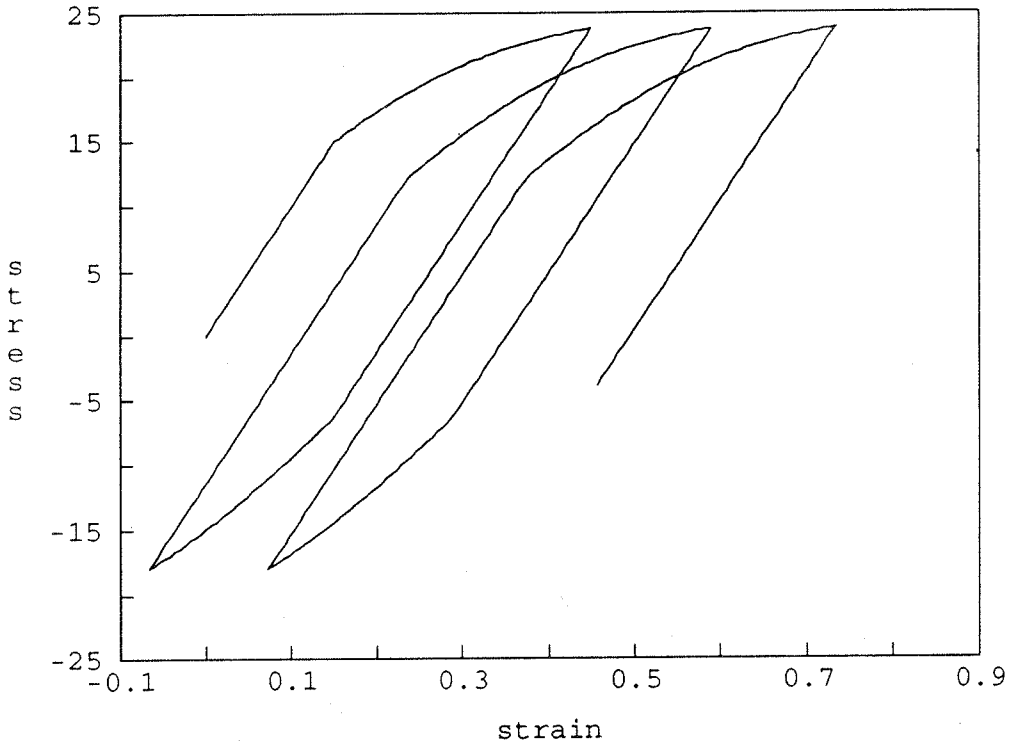

Figure 21: Non-linear kinematic hardening model (NLK) under cyclic uni-axial load (force control, non-zero mean stress). Uni-axial stress σ versus uni-axial strain ϵ.
$\sigma^u_{y,0} = 15$, $H^u_{kin} = 100$, $H^u_{nl} = 10$, $H^u_{iso} = 0$

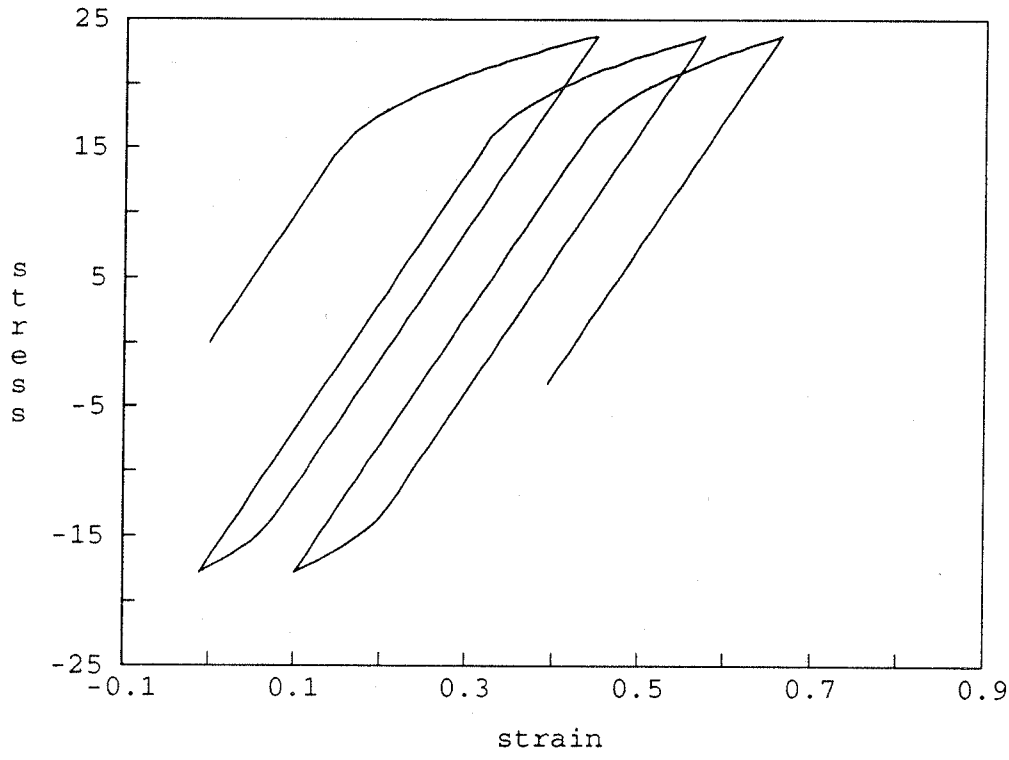

Figure 22: Generalized plasticity (GP) under cyclic uni-axial load (force control, non-zero mean stress). Uni-axial stress σ versus uni-axial strain ϵ. $\sigma^u_{y,0} = 15$, $\beta^u = 20$, $\delta^u = 5$, $H^u_{kin} = 5$, $H^u_{iso} = 0$.

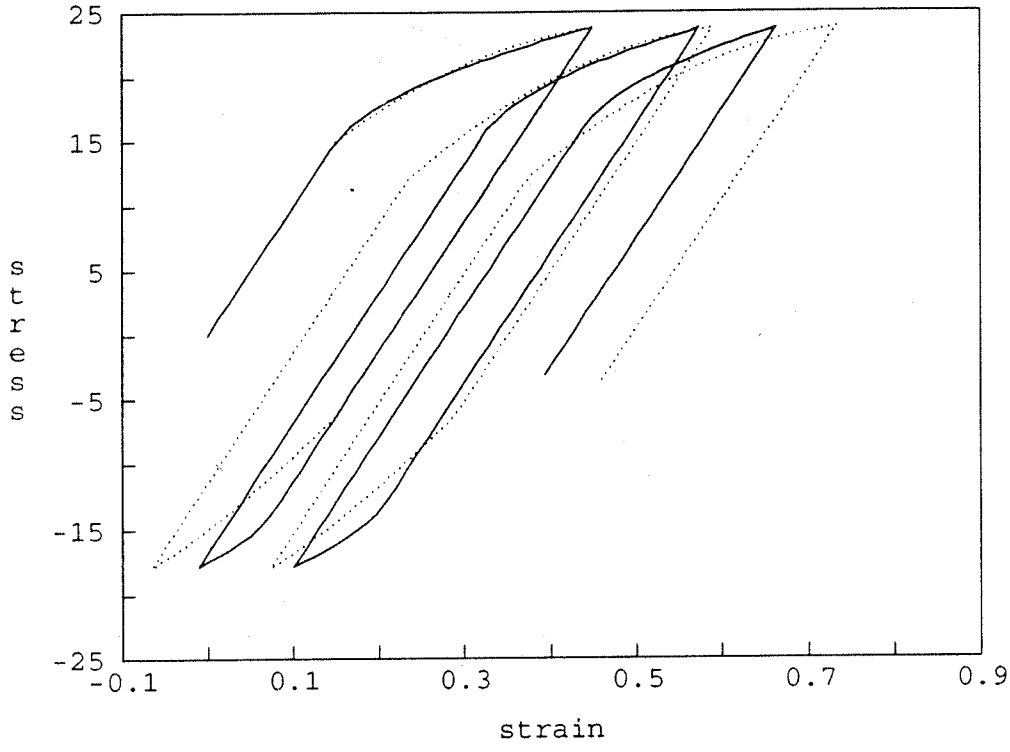

Figure 23: Generalized plasticity (GP) [continuous line] versus non-linear kinematic hardening (NLK) [dotted line] under cyclic uni-axial load (force control, non-zero mean stress). Uni-axial stress σ versus uni-axial strain ϵ.

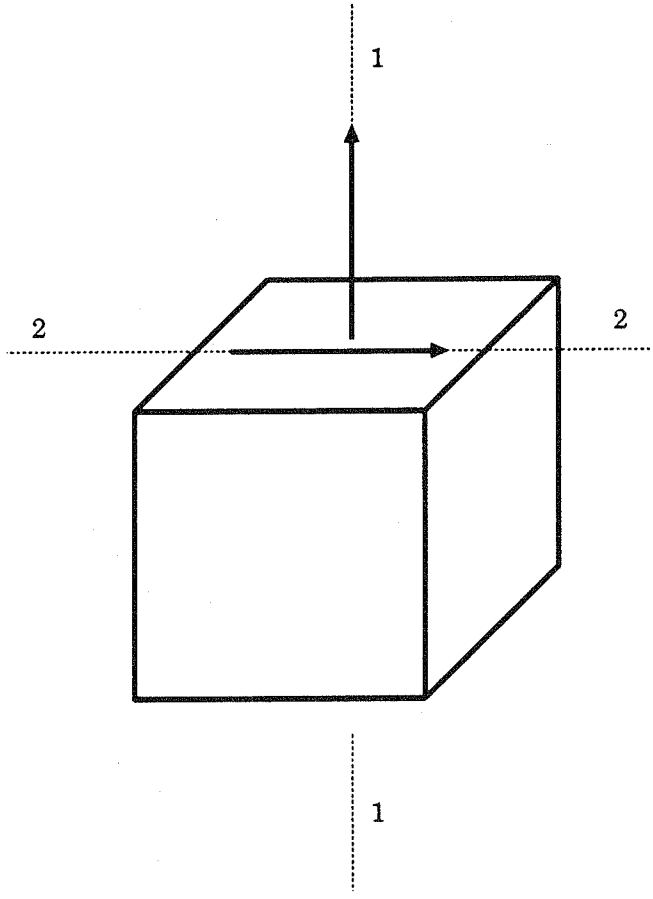

Figure 24: Specimen adopted for the tension-cyclic shear test. Tension applied in the 1-1 direction, shear applied in the 1-2 direction.

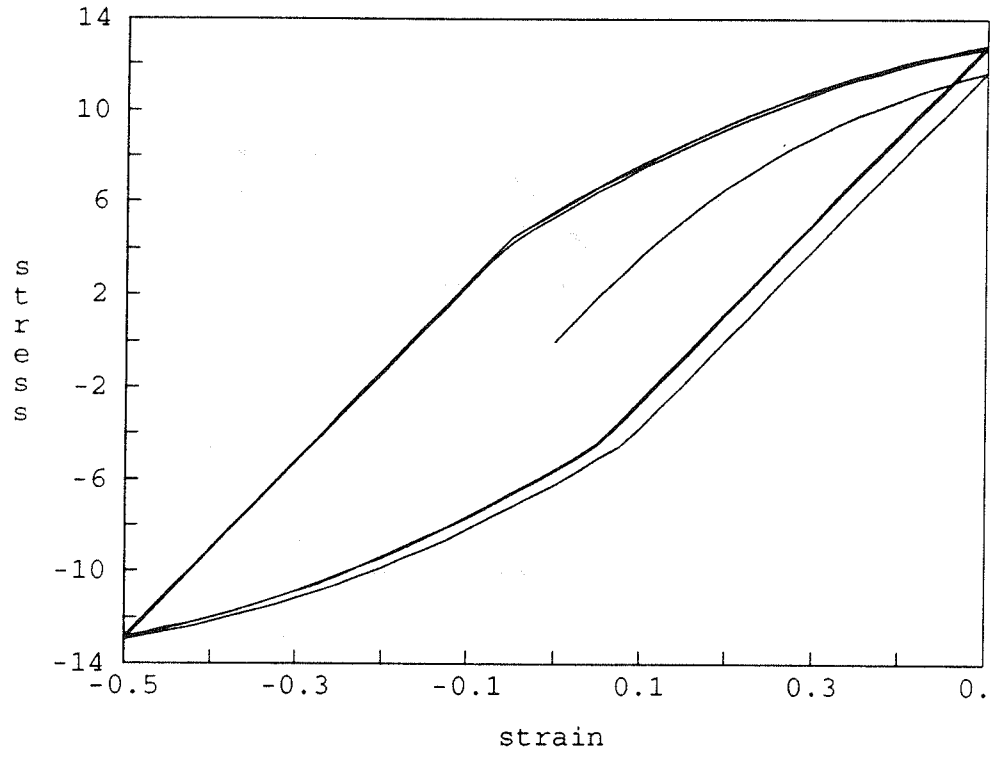

Figure 25: Non-linear kinematic hardening model (NLK) under tension-cyclic shear (displacement control). Shear stress τ_{12} versus shear strain γ_{12}.
$\sigma^u_{y,0} = 15$, $H^u_{kin} = 100$, $H^u_{nl} = 10$, $H^u_{iso} = 0$

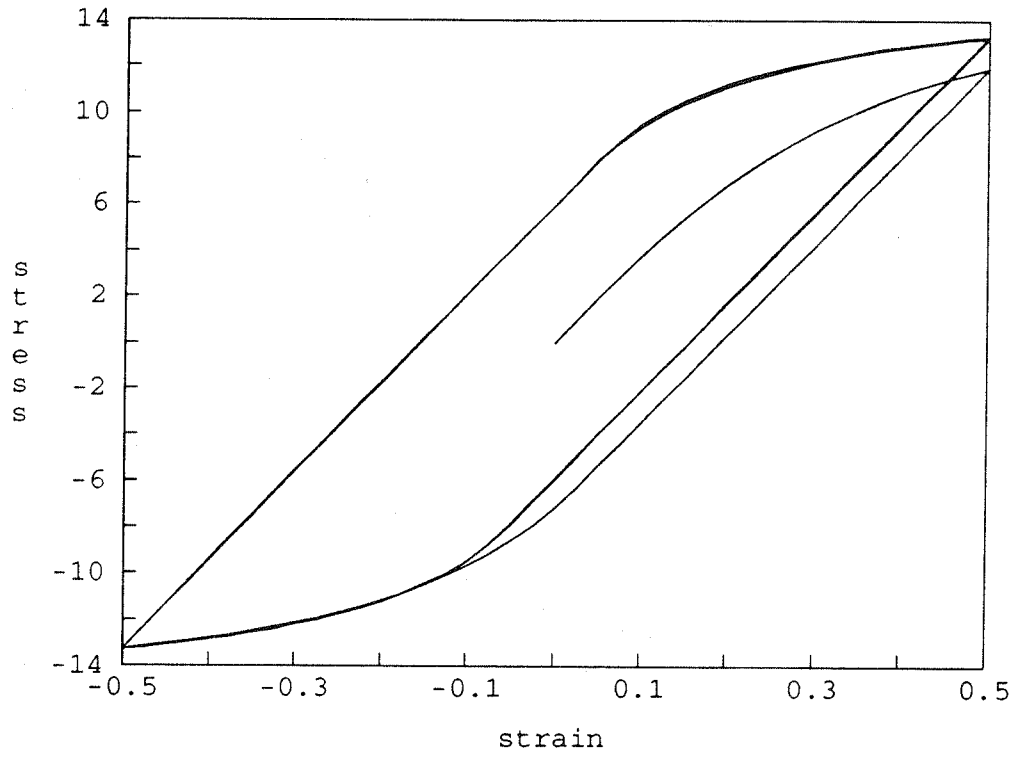

Figure 26: Generalized plasticity (GP) under tension-cyclic shear (displacement control). Shear stress τ_{12} versus shear strain γ_{12}.
$\sigma^u_{y,0} = 15$, $\beta^u = 10$, $\delta^u = 50$, $H^u_{kin} = 0$, $H^u_{iso} = 0$.

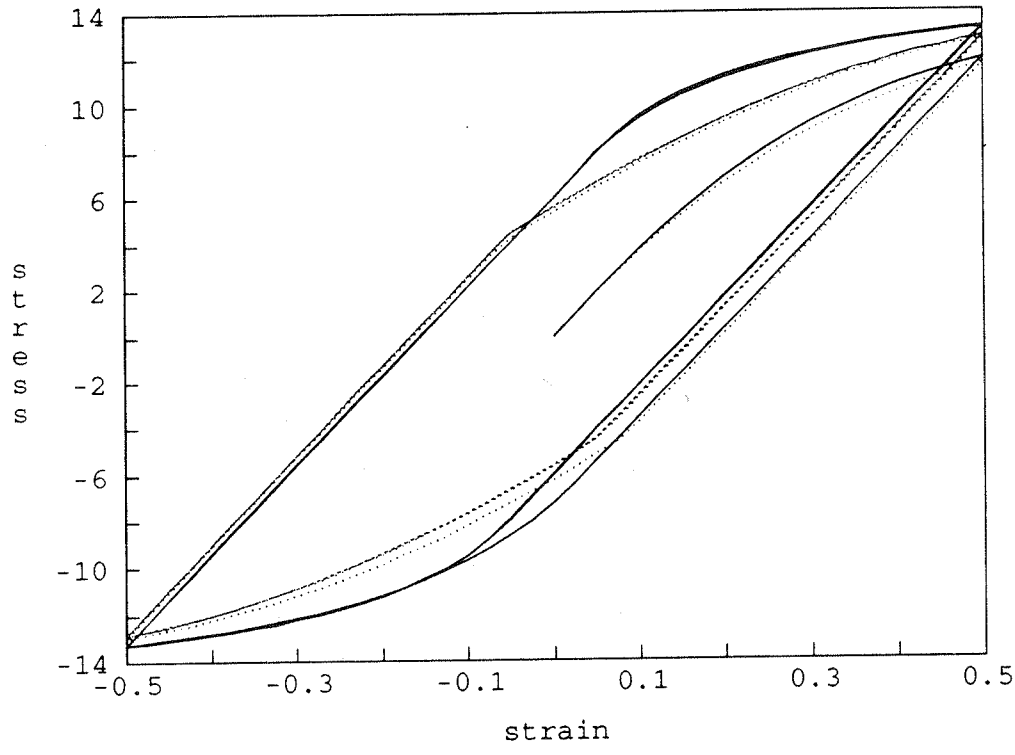

Figure 27: Generalized plasticity (GP) [continuous line] versus non-linear kinematic hardening (NLK) [dotted line] under tension-cyclic shear (displacement control). Shear stress τ_{12} versus shear strain γ_{12}.

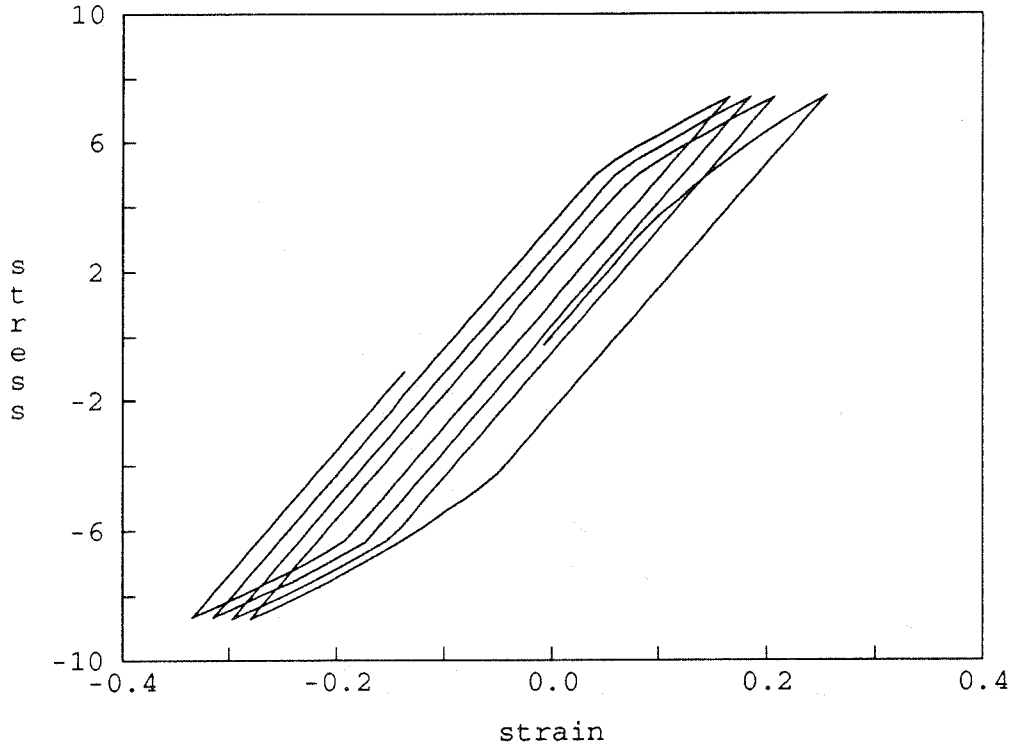

Figure 28: Non-linear kinematic hardening model (NLK) under tension-cyclic shear (force control). Shear stress τ_{12} versus shear strain γ_{12}.
$\sigma^u_{y,0} = 15$, $H^u_{kin} = 100$, $H^u_{nl} = 10$, $H^u_{iso} = 0$

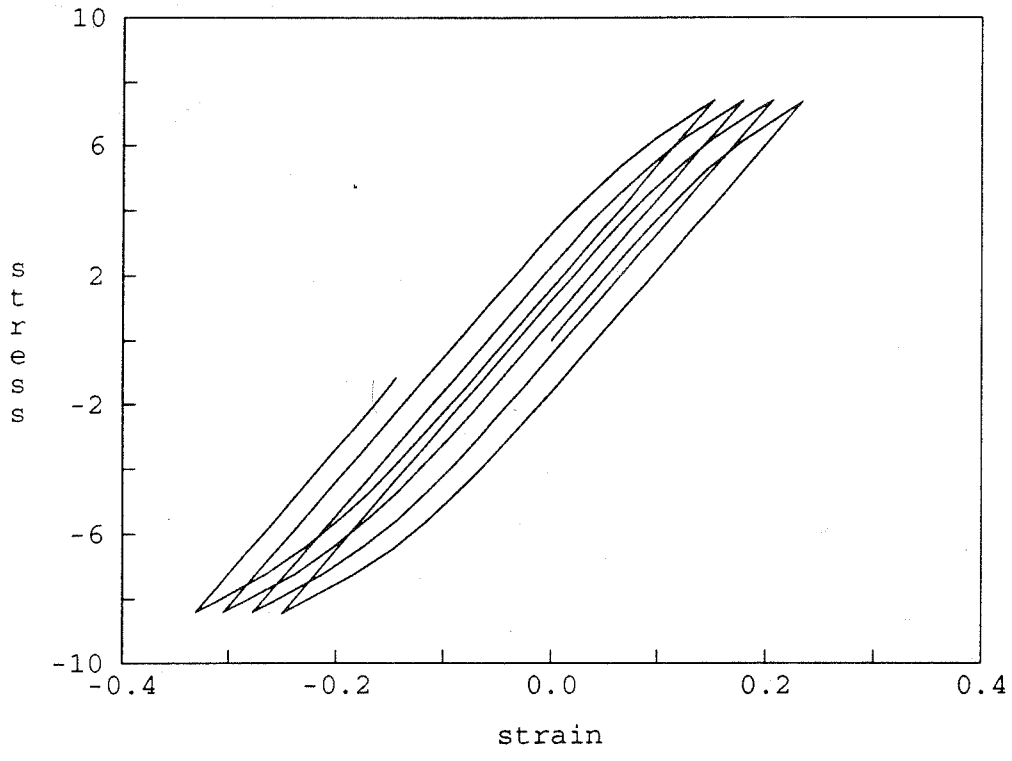

Figure 29: Generalized plasticity (GP) under tension-cyclic shear (force control). Shear stress τ_{12} versus shear strain γ_{12}.
$\sigma^u_{y,0} = 15$, $\beta^u = 10$, $\delta^u = 50$, $H^u_{kin} = 0$, $H^u_{iso} = 0$.

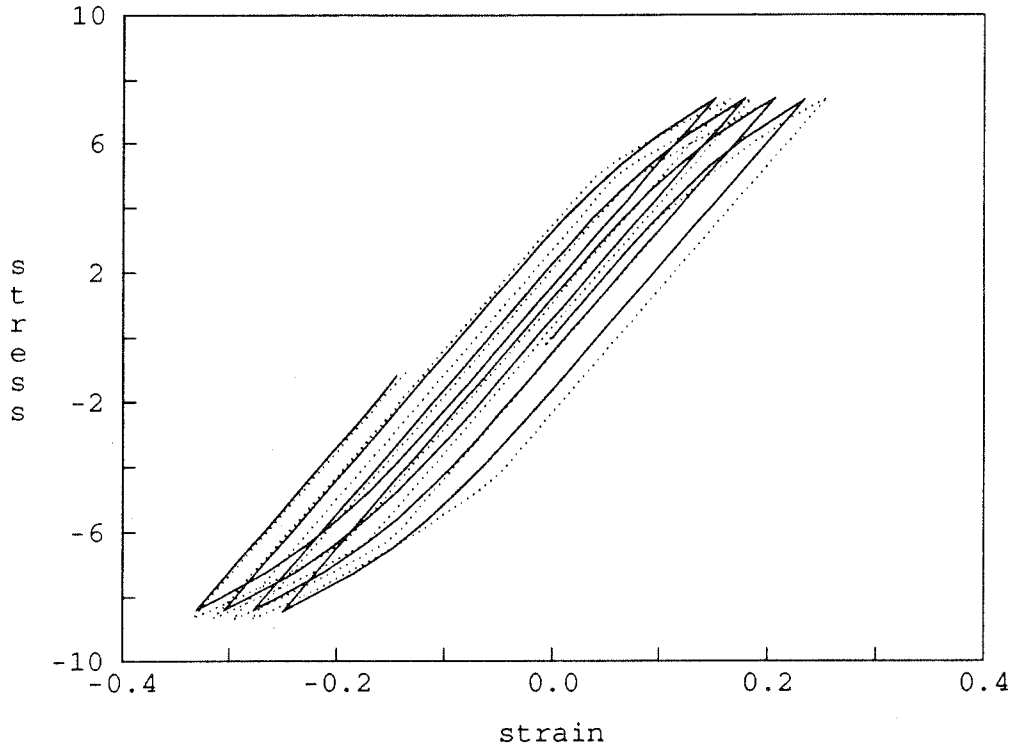

Figure 30: Generalized plasticity (GP) [continuous line] versus non-linear kinematic hardening (NLK) [dotted line] under tension-cyclic shear (force control). Shear stress τ_{12} versus shear strain γ_{12}.